

# Periods and classifications of RR Lyrae stars in the globular cluster M15

Andrew M. Hoffman,<sup>1,2,3</sup>★ Yukei S. Murakami,<sup>1,2,3</sup>†

WeiKang Zheng,<sup>1</sup> Benjamin E. Stahl,<sup>1,2,4</sup> and Alexei V. Filippenko<sup>1,5</sup>

<sup>1</sup>*Department of Astronomy, University of California, Berkeley, CA 94720-3411, USA*

<sup>2</sup>*Department of Physics, University of California, Berkeley, CA 94720-7300, USA*

<sup>3</sup>*Google Lick Predoctoral Fellow*

<sup>4</sup>*Marc J. Staley Graduate Fellow*

<sup>5</sup>*Miller Senior Fellow, Miller Institute for Basic Research in Science, University of California, Berkeley, CA 94720, USA*

Accepted to MNRAS (December 2020).

## ABSTRACT

We present measurements of the periods, amplitudes, and types of 74 RR Lyrae stars in the globular cluster M15 derived from Nickel 1 m telescope observations conducted at Lick Observatory in 2019 and 2020. Of these RR Lyrae stars, two were previously reported but without a determination of the period. In addition, we identify five Type II Cepheid variable stars for which we report three novel period determinations, and a further 34 stars with uncertain classifications and periods. We discuss the development and subsequent application to our data of a new Python package, Period-determination and Identification Pipeline Suite (PIPS), based on a new adaptive free-form fitting technique to detect the periods of variable stars with a clear treatment of uncertainties.

**Key words:** globular clusters: individual (M15) – stars: evolution – stars: variables: RR Lyrae – methods: data analysis – techniques: photometric

## 1 INTRODUCTION

Pulsating variable stars periodically change their brightness over timescales ranging from a few minutes to a few months, making them members of a select group of astronomical objects that are dynamic over time intervals that are observable by humans (for a review, see, e.g., Percy 2007). Moreover, the observable details of this dynamic behaviour follows patterns that are unique to each type of variable star, a property that makes photometric time-series analysis a particularly useful tool for their study (Budding & Demircan 2007).

The astrophysical applications of variable-star observations span many fields, such as testing hydrodynamical models (Smolec & Moskalik 2012) and investigating the expansion of the Universe (Scolnic et al. 2019, and references therein). If the measurements of a variable star’s parameters are uncertain, this error can propagate into many other “downstream” facets of an analysis — accuracy is, therefore, critical.

RR Lyrae variable stars are evolved low-mass stars which have moved off the main sequence onto the horizontal branch. They are among the most common types of variable stars in Galactic globular clusters (Clement et al. 2001). Despite a large number of samples

and a long history of observations (from Pickering et al. 1901 to, e.g., Pietrukowicz et al. 2020), the behaviour of RR Lyrae stars is not fully understood. For instance, the expected long-term behaviour of the period is not agreed upon nor immediately evident in observations. Stars do not remain on the horizontal branch forever (Jurcsik et al. 2003), but the degree, timescale, and type of evolution within the branch are not trivial to theorise or measure. Observations spanning large temporal ranges ( $\sim 100$  yr) suggest that RR Lyrae stars have generally stable periods (Arellano Ferro et al. 2018), but some theories predict noticeable changes (Fadeyev 2018). Moreover, the short-term modulation of light curves (Blažhko 1907) seen in some stars remains an open question. Recent studies (Szabó et al. 2014) suggest that the multimode property of such “Blazhko stars” resembles known multimode RR Lyrae stars (RRd), and studies connecting them are needed.

When investigating RR Lyrae stars it is valuable for repeated observations to be made as often as possible. Such data yield (among other things) a basis with which to investigate long-term changes and may yield insights into tricky phenomena such as multimode pulsations and the Blazhko effect. Messier 15 (NGC 7078, M15) is well suited for such studies. It is an old and star-dense globular cluster (Mészáros et al. 2020) that contains many evolved star types, and in particular, dozens to hundreds of RR Lyrae stars which can be well resolved by telescopes of moderate size. Many photometric observations of RR Lyrae stars in M15 can be found in the literature,

★ E-mail: andrewmh@berkeley.edu

† E-mail: sterling.astro@berkeley.edu

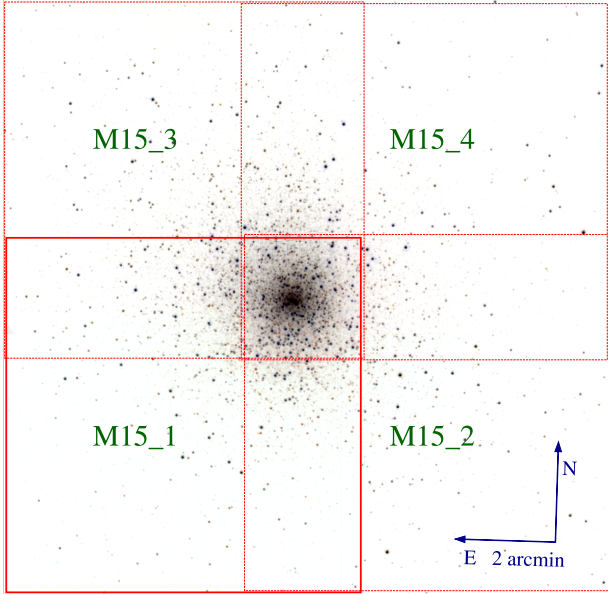


**Figure 1.** Tiled images of M15, with each being a *BVR* composite of inverted-color Nickel telescope images. Our observations cover  $10' \times 10'$  centred at the core of M15 by combining four tiled images (M15\_1 – M15\_4) that each have a  $\sim 6' \times 6'$  field. Note the slight rotation ( $\sim 1.5^\circ$ ) of the compass rose.

including Bailey et al. (1919), Wemple (1932), Mannino (1956), Makarova & Akimova (1965), Sawyer Hogg (1973), Filippenko & Simon (1981), Bingham et al. (1984), Silbermann & Smith (1995), Corwin et al. (2008), Arellano Ferro et al. (2006), and Siegel et al. (2015).

In this paper, we present new observations of RR Lyrae stars in M15 and an analysis of their types and pulsation periods. In Section 2 we describe our observations and data-processing methods. We also discuss matching the variable stars detected from raw data with known catalogued variable stars. Section 3 describes our method of detecting the period of observed variable stars, with an emphasis on dealing with widely spaced data, and also discusses our methods of handling error propagation and star classification. In Section 4 we present the periods, magnitudes, and type classification of 74 RR Lyrae stars recovered from our observations and derived by our analysis. We also highlight several stars for which few or no previous detections exist, discuss a number of additional stars for which we were not able to accurately determine periods, and briefly describe period determinations for a small number of Type II Cepheid variable stars. We give conclusions and directions for future work in Section 5.

## 2 OBSERVATIONS AND DATA REDUCTION

### 2.1 Observations

Over approximately one year, we obtained 691 images of M15 on 46 nights using the Nickel 1 m telescope, located at Lick Observatory (Mt. Hamilton, CA). We observed M15 for an average of 20 min per night, on nights devoted mainly to supernova photometry, with a typical time between observations of roughly 7 d. As RR Lyrae stars generally have oscillation periods of 0.2–0.9 d (Corwin et al.

2008), our observing cadence produces widely scattered data when compared to the pulsation period. Ideally, fast pulsators such as RR Lyrae stars should be observed as often as possible to capture the full range of behaviour (VanderPlas 2018). With widely scattered data, period determination becomes difficult, as does avoiding aliasing.

After considering the field of view of the Nickel telescope, we chose to take 4 tiled fields of M15 in order to image the largest number of stars. The arrangement is shown in Figure 1. Specific locations of variable stars within these fields can be found in Figures B10–B13. Our typical observations of a given field consisted of exposures of 20, 60, and 180 s in the *V* band, generally three times per night. This strategy increases the likelihood of obtaining at least one data point per night with a sufficiently high signal-to-noise ratio (SNR), given the varying brightness of our targets. When time permits, images were also taken in the *B* band.

With a plate scale of  $0.368'' \text{ pixel}^{-1}$  after binning<sup>1</sup>, and a median seeing of  $(2.02 \pm 0.50)''$ , the core of M15 is sometimes not well resolved in our images. Because of this, there are limitations in period determinations for stars which are located close to the core due to possible contamination and blending. When examining previously published data, we see a similar trend where stars which are harder to individually resolve are less likely to have reported periods (e.g., Siegel et al. 2015). To minimise the effect of this issue, tiled fields are overlapped at the core, increasing the chance of detection by collecting a larger number of data points. Although outside the scope of this work, higher resolution images of M15 (such as Hubble photometry e.g., Sarajedini et al. 2019) exist, which can help distinguish between stars in these dense regions.

### 2.2 Data Reduction

#### 2.2.1 LOSSPhotPipeline

We utilise the LOSSPhotPipeline<sup>2</sup> (LPP; Stahl et al. 2019) to perform photometry on the images taken from the Nickel telescope and construct light curves in the Nickel2 natural system. The LPP provides robust methods for uncertainty calculation, including reduction on simulated stars in the field. We use these uncertainties as a proxy by which to identify poor-quality data that need to be removed from further analysis. As our use of the LPP is consistent with that of Stahl et al. (2019), we defer to their Section 3 for a more detailed discussion of its capabilities.

#### 2.2.2 Calibration

We calibrate each field by picking bright, nonvariable stars that have minimal (typically  $< 0.03 \text{ mag}$ ) deviation from the corresponding PS1 catalogue values, converted to the Landolt-system (Landolt 1983, Landolt 1992) using the prescription of Tonry et al. (2012), and then to the Nickel2 natural system using the transformations and color terms presented by Stahl et al. (2019), and small (also typically  $< 0.03 \text{ mag}$ ) scatter (per calibration star) in each of their observed magnitudes through the entire time series. The first criterion ensures calibration consistency between the four different fields in our tiling strategy (see Fig. 1), and the second — in conjunction with the requirement that only those calibration stars that are detected in every image for a given field be used — ensures a

<sup>1</sup> We use  $2 \times 2$  binning with the  $2048 \times 2048$  CCD whose normal plate scale is  $0.184'' \text{ pixel}^{-1}$ .

<sup>2</sup> <https://github.com/benstahl192/LOSSPhotPipeline>

**Table 1.** Statistics for calibration stars used in each field.  $N_{\text{stars}}$  is the number of calibration stars in each field.  $\Delta V$  is the deviation from the corresponding PS1 magnitude and  $\sigma V$  is the observed standard deviation, both in the  $V$  band.

Field	$N_{\text{stars}}$	$\overline{\Delta V}$ (mag)	$(\Delta V)_{\text{max}}$ (mag)	$\overline{\sigma V}$ (mag)	$(\sigma V)_{\text{max}}$ (mag)
M15_1	9	-0.0002	0.0242	0.0170	0.0319
M15_2	9	-0.0004	0.0157	0.0162	0.0303
M15_3	8	-0.0004	0.0346	0.0218	0.0340
M15_4	10	-0.0012	0.0210	0.0192	0.0245

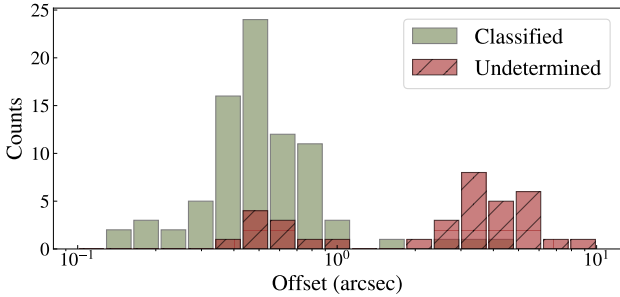


**Figure 2.** Offset of our candidate stars from GCVS catalog  $\theta_i$ , in arcsec. Successful classifications tend to correlate with a small offset.

consistent calibration for images taken across long time intervals. This calibration process introduces scatter in our data. The characteristic value of this scatter for combined fields can be calculated from the mean and maximum standard deviation of calibration star magnitudes  $\overline{\sigma V}$ . We see a characteristic value of  $\langle \overline{\sigma V} \rangle \approx 0.02$  and  $\langle (\sigma V)_{\text{max}} \rangle \approx 0.03$ , which is representative of the uncertainty of our measurements. Considering the characteristic uncertainty in our data, we set a 0.03 mag floor on magnitude uncertainties (commensurate with our second criterion). We summarise important statistics for our calibration choices in Table 1, while detailed information is relegated to Table A2 in the Appendix. Unless otherwise noted, we do not accept data above an uncertainty threshold  $\sigma_V \geq \sigma_{V,\text{cut}}$ , where  $\sigma_{V,\text{cut}} = \overline{\sigma V} + \text{std}(\sigma_V)/2$  for each star.

### 2.2.3 Cross-matching

We identify candidate variable stars using the LPP’s ability to automatically detect all resolvable stars in an image. For each field, this procedure identifies  $\sim 1300$  candidates, which we then compare to previously published positions for variable stars. Specifically, we calculate the angular distance between star  $i$  identified by the LPP and star  $j$  in Samus’ et al. (2017, hereafter GCVS),  $\theta_{ij} = \cos^{-1} [\sin(\delta_i) \sin(\delta_j) + \cos(\delta_i) \cos(\delta_j) \cos(\alpha_i - \alpha_j)]$ . Here,  $\alpha$  is the right ascension and  $\delta$  is the declination of the subscripted object, both in radians. Once this two-dimensional array is generated, we take  $\min(\theta_j)_i$  to create a list of the variable stars nearest to each candidate. This list contains many duplicates, so we further narrow it by taking  $\min(\min(\theta_j)_i)_j$  for each duplicate star  $j$ . The resulting list contains each star’s coordinates ( $\alpha$  and  $\delta$ ), identification (ID), and the offset from the relevant GCVS star. This process is repeated for all four fields, M15\_1 to M15\_4. Our star ID is expressed with “V” numbers (e.g., V001). This is a slightly modified version of older notations, such as VI, as seen in Bailey (1902) and

other papers. After this process, we obtain  $\sim 60$  candidate stars in each field to be processed.

Since there are overlaps between each field, we process stars in more than one field whenever possible, thereby allowing us to choose the data based on various quality parameters (see Sec. 3.1). The resulting, cross-matched catalogue shows strong agreement with GCVS coordinates. There are two populations, one with a small ( $\sim 0.4''$ ) offset and one with a larger ( $\sim 2.5''$ ) offset, which are visible in Figure 2. Our final selections (see Sec. 4) suggest that stars in the second (large-distance) population mostly fail to provide high-quality data. Assuming GCVS has high accuracy, this is the expected result. Note that while most of our successfully classified stars fall in this “low offset” population, the offset value  $\theta_i$  is used only for cross-matching candidates, and our final classification is based on photometric results (see Sec. 4).

## 3 ANALYSIS

### 3.1 PIPS

We have developed the Period-determination and Identification Pipeline Suite (PIPS)<sup>3</sup>, a new Python package to analyse variable-star data. While there are many algorithms and code bases available for this purpose, we found that several improvements were needed to obtain the best results, especially for difficult objects characterised by widely spaced data, low SNR, and few data points.

#### 3.1.1 Motivation and Background

**Period Uncertainty** — We note that in older publications, particularly in studies which rely on the time of maximum light (see, e.g., Bailey 1902; Wemple 1932; Makarova & Akimova 1965), uncertainty quantification is not treated carefully. More recently, the method of fitting to folded data instead of relying on the maximum or minimum times has become more prominent (see Holl et al. 2018), and with it, a clearer understanding and treatment of uncertainty. This is of great importance for modern studies as long-term data can and will be used to study the evolution of certain quantities (e.g., period and metallicity), and a careful treatment of uncertainty is required for proper error propagation and the statements of confidence that such calculations support. In developing PIPS, our primary concern was therefore to examine the uncertainty created when making period determinations.

**Template Bias** — When analysing variable-star photometry, our goal is to determine the period and create analytic functions (e.g., Fourier series) which provide an accurate description of the star’s light curve. Although high-cadence observations can yield a complete light curve and through it, a direct measurement of the period, data are often<sup>4</sup> taken with a lower cadence which does not immediately show a clear morphology — this is indeed the case with our data. This necessitates a phase-folded light curve (VanderPlas 2018), and therefore requires a determination of the period before analysis can proceed. The principal challenge in our work is then to make accurate period determinations, and hence, construct accurate phase-folded light curves.

The Lomb-Scargle periodogram is the most common algorithm designed to detect sinusoidal signals in widely or unevenly

<sup>3</sup> <https://github.com/SterlingYM/PIPS>

<sup>4</sup> For instance, in many modern all-sky surveys.

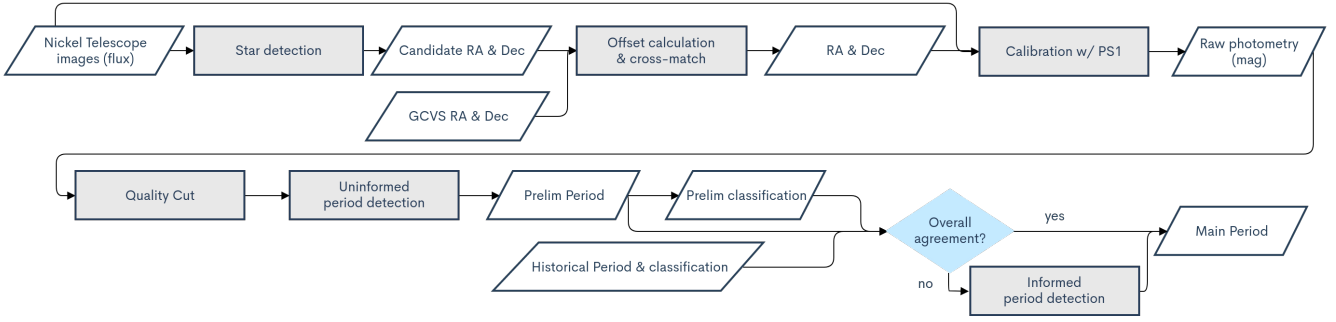


**Figure 3.** Data-reduction process chart.

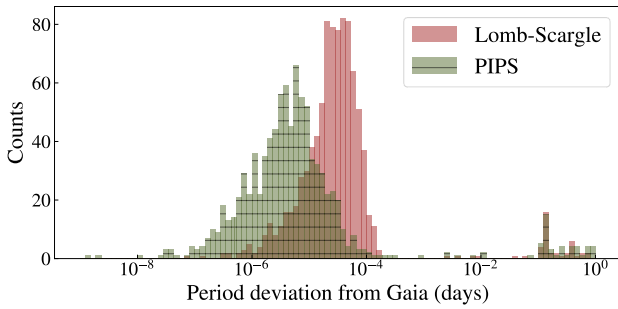


**Figure 4.** Deviation from Gaia period ( $\Delta P$ ) when analysed with Lomb-Scargle (red) and PIPS (green).

spaced data (VanderPlas 2018). Template Fourier Fitting (TFF; Kovács & Kupi 2007) is a technique which leverages high-cadence data of similar phenomena to create an informed prior for light-curve fitting. Both of these techniques can make period determinations, but the bias induced by one’s choice of light-curve template is not widely addressed.

Owing to Lomb-Scargle’s nature as a correlation function to a sinusoidal pattern (Lomb 1976; Scargle 1982), taking the maximum returned power value only yields the best-fit period to a sinusoidal wave. Because the higher order terms of a Fourier fitting do not always have negligible amplitude, this sinusoidal dependence is analogous to the template dependence in TFF. Both the template dependence in TFF and the sinusoidal dependence in LS skew results from these methods. The RRab type of RR Lyrae stars, for instance, have sharply peaked maxima which are poorly described by a sinusoid (e.g., light curves in Filippenko & Simon 1981; Corwin et al. 2008). For this reason, we employ a template-free fitting method with PIPS to minimise bias.

### 3.1.2 Methodology

PIPS is a period-determination algorithm based on template-free, adaptive-function (“Free-Form”) fitting. The analysis begins with an initial guess from the Lomb-Scargle periodogram, but proceeds to refine the value and explore the associated uncertainty. We assume that when a light curve is folded about a more correct period, fitting will yield a smaller  $\chi^2$  value compared to a folding about a value farther from the true pulsation period. We also assume that there will be one global minimum when examining the  $\chi^2$  space, representing the true period of the star. The simplest way to find

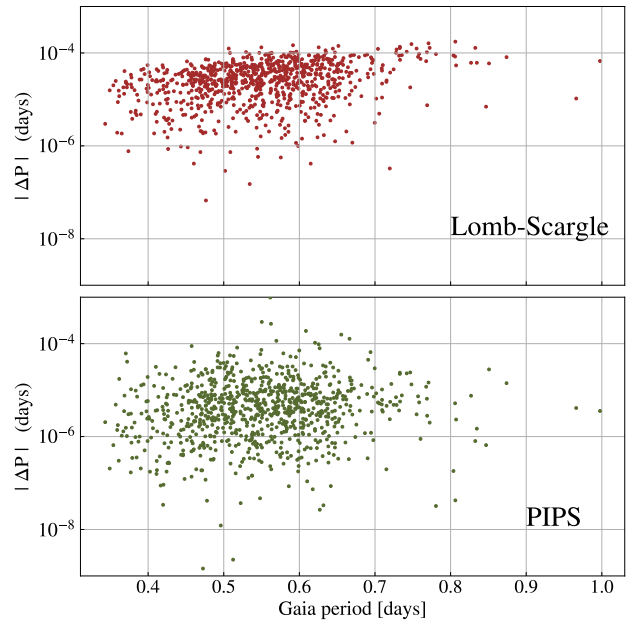


**Figure 5.**  $|\Delta P|$  as a function of Gaia’s period, for our stars with  $\Delta P < 10^{-2}$  only. Lomb-Scargle shows a slight correlation between period and error, while our pipeline is more consistent across a large range of periods.

this correct period would be to iterate through the entirety of possible periods and perform a fit to the data folded with each period in turn. This is computationally intensive, inefficient, and complicates the exploration of uncertainty. We choose instead to provide an informed prior based on the Lomb-Scargle estimation, and use  $\chi^2$  minimisation where both the period and the Fourier terms are free parameters. We find that this identifies the period more accurately and that this exploration of parameter space provides robust information regarding the uncertainty of the value.

Given time-series data, PIPS finds the best value for the principal pulsation period by checking  $\chi^2$  values against the best-fit Fourier function which represents the analytic form of the light curve,

$$y_{\text{fit}} = A_0 + \sum_{k=i}^{K_{\text{max}}} \left[ a_k \cos\left(\frac{2\pi k}{P}x\right) + b_k \sin\left(\frac{2\pi k}{P}x\right) \right]. \quad (1)$$

Here,  $x$  is the phase-folded time data  $x \equiv t \pmod{P}$ , and  $y_{\text{fit}}$  represents the expected magnitude at that phase (the unitless phase



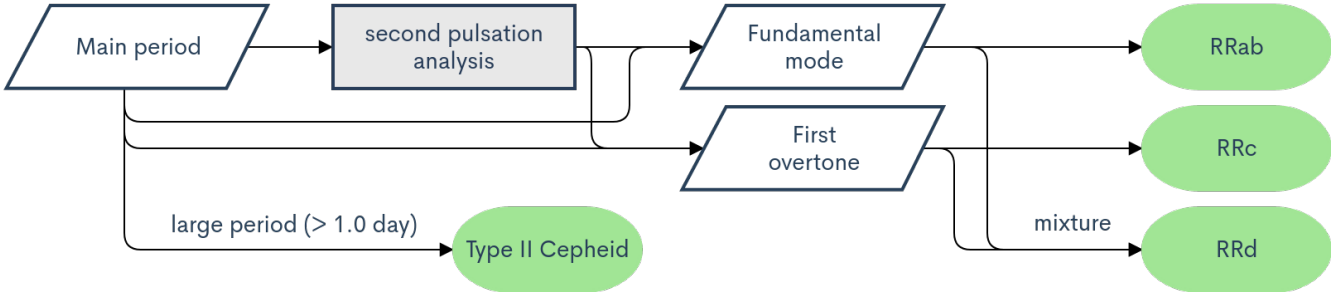


**Figure 6.** A flowchart showing the procedure to classify variable stars.

is  $x/P$ ). The parameters  $A_0$ ,  $a_k$ ,  $b_k$ , and  $P$ , are determined by a linear-regression fitting using the `curve_fit` function in `scipy` (Virtanen et al. 2020). In this analysis, we take  $K_{\max} = 5$ , based on a cross-validation test using Gaia data of RR Lyrae stars.

The number of parameters and intrinsic scatter (or a small SNR) may in some cases make it difficult to fit the correct value of  $P$ . This is primarily because Fourier parameters dominate the degrees of freedom, yielding many local minima in the  $\chi^2$  space when viewed as a function of  $P$ . Additionally, the change in the  $\chi^2$  value at different  $P$  becomes less obvious as the SNR decreases, because even at the best  $P$ , the folded data exhibit a roughly correct shape but with large intrinsic scatter, yielding a relatively large  $\chi^2$  value. These relations can be viewed as analogous to the mechanics of a potential well whose surface is the representation of the  $\chi^2$  value. This well exhibits a larger friction force between sliding objects as the surface becomes rougher (many local minima) due to different combinations of Fourier coefficients. The SciPy `curve_fit` function attempts to “place an object” (the initial guess) to perform tests with the goal of finding the “bottom” of the well. How far this test object slides down is a function of the slope. This “slide test” tends to be unsuccessful near the bottom of the potential, which can be seen in a nearly one-to-one relationship between the initial guess and the resulting “best fit” period. The “initial kick” from the linear regression algorithm yields a characteristic size in the scatter of the resulting period when compared to the initial guess values, and we take this as the statistical uncertainty of the period<sup>5</sup>

$$\sigma_P = \text{std}(P_{\text{fit}} - P_{\text{trial}}) \Big|_{P_{\text{trial}} \approx P}. \quad (2)$$

This process requires a fitting to Equation 1 between  $10^2$  and  $10^4$  times, and our pipeline is designed to perform this analysis as fast as possible. When the uncertainty of the period is not required, it is sufficient and much faster to find the  $P$  value which yields a minimum  $\chi^2$  for Equation 1 when evaluated as a function of  $P$  (i.e., fixed  $P$  within single fitting).

### 3.1.3 Performance Validation

We tested the period-detection function of our pipeline with raw RR Lyrae light curves from Gaia DR2 (Holl et al. 2018). We chose a sample consisting of 1355 RR Lyrae stars (`gaiadr2.vari_rrlyrae`). This set of data includes 910 RRab stars and 445 RRc or RRd stars, whose photometry in the  $G$  band is

taken for more than 30 epochs (`num_clean_epochs_g > 30`) and is located nearby (`parallax > 0.25`) with less than 20% uncertainty in its astrometry measurement (`parallax_over_error > 5`). We search for any period between 0.2 and 1.0 d equally without an initial guess, with no visual inspection or human help.

The results for this validation are shown in Figures 4 and 5. In most cases both Lomb-Scargle (LS) and PIPS agreed with Gaia’s period, although there is a population with  $\sim 0.1$ – $1.0$  d error in period values. About 96% of LS results and 95% of PIPS results were considered “good results,” and PIPS outperforms LS with mean error an order of magnitude smaller than LS results. Moreover, LS exhibits a slight correlation between  $\Delta P$  and period, an expected behaviour when a noninformed uniform prior in frequency space is used. This creates unequally-spaced windows in period space and thus the resolution becomes lower as the period increases. PIPS adaptively changes the search-window size, and therefore does not exhibit this issue.

Since Lomb-Scargle is a widely accepted tool in the community, we consider our new package PIPS as an equally acceptable tool overall and one which may be better suited for our particular analysis based on these validation results.

## 3.2 Classification

RR Lyrae stars are generally classified based on their pulsation modes. This classification was first introduced by Bailey (1902) based on morphology, and other than the consolidation of RRA and RRb stars into the RRab type, it has remained the accepted method. Although RR Lyrae stars as a group span a huge range of behaviors, within our sample we see that our RR Lyrae types are largely separated by the fundamental mode pulsation, with RRab (also called RR0) having a 0.5–0.7 d period and the first-overtone pulsation, RRc (RR1), having a  $\sim 0.3$  d period. Some stars exhibit a combination of these two modes, and are classified as RRd (RR01). The fundamental mode generally has a steep rise in magnitude, while the first overtone is closer to a sinusoid. The shapes of these light curves can be explained using sophisticated hydrodynamical calculations (see Stellingwerf (1975), Kolláth et al. (2002)). Some RR Lyrae stars may exhibit significant modulations in amplitude, phase, and period over a few days (Jurcsik et al. 2006) to several years (Prudil & Skarka 2017). This phenomenon is called the “Blazhko effect” after the first observation (see Blažko 1907), and several attempts have been made to explain it (Smolec 2016). The more complex simultaneous modulations of amplitude and period are always present in Blazhko RRab stars (See Benkő et al. 2010). Modulations can also be seen in RRc stars, primarily (but not exclusively) in amplitude.

In order to classify the stars in our sample, we follow the

<sup>5</sup> Here, we use  $\text{std}(x)$  as a short notation for the standard deviation,  $\text{std}(x) = \sqrt{[\sum_i^N (x_i - \bar{x})^2] / N}$ .

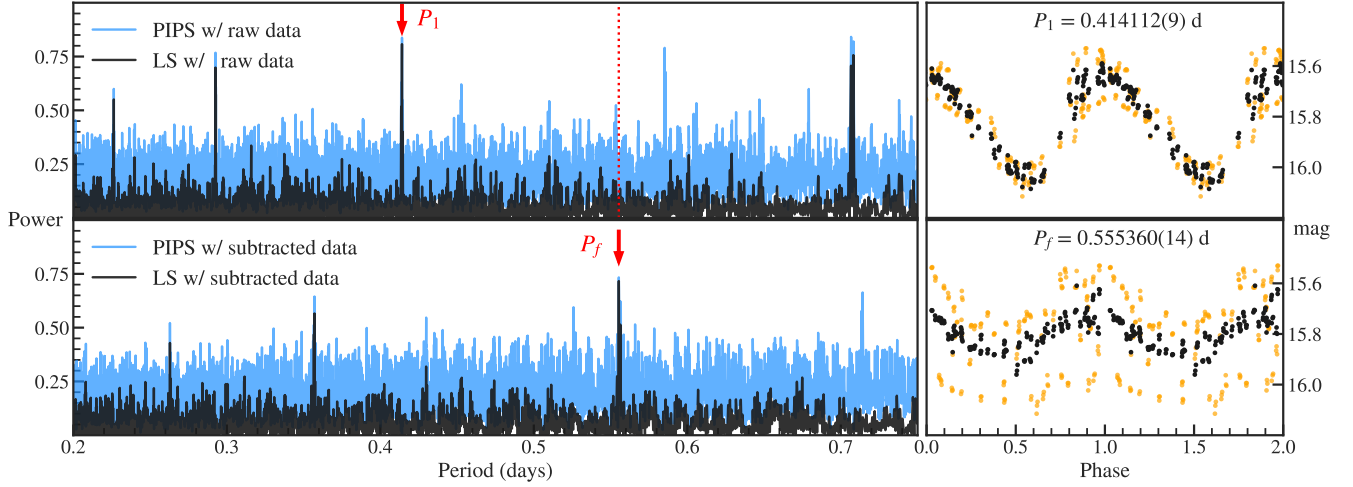


**Figure 7.** Left: Periodograms created for the intermediate steps in RRd classification. Blue (lighter color) represents the normalized periodogram created by PIPS and the black (darker color) represents the Lomb-Scargle periodogram. The power values in PIPS periodogram are compared with  $\chi^2$  values evaluated against Eq.1,  $\mathcal{P} = 1 - \chi^2/\chi_0^2$ . Here,  $\chi_0^2$  is the non-varying reference  $\chi_0^2 = \sum (y_i - \bar{y})^2/\sigma_i^2$ . Right: Decoupled modes at each detected period. Orange (lighter color) represents the raw data folded at each period, without subtraction. The abscissa represents the dimensionless phase (repeated twice).

general methodology seen in most RR Lyrae star and M15-specific studies (e.g., Silbermann & Smith 1995; Clementini et al. 2016). Although the original method to distinguish between RRAb and RRC stars is morphology-based and requires a careful statistical study of population and various parameters, it is now clear that RRAb stars can be distinguished from RRC and RRd stars clearly in period space. This is especially true in M15, whose member objects share similar metallicities and ages (Mészáros et al. 2020). This prior knowledge about a narrow range of metallicities resolves the possible degeneracy that arises between different Oosterhoff groups (Oosterhoff 1939).

Our procedure to classify variable stars follows three steps: (1) based on existing studies, we confirm that the distribution of our detected periods agrees with those in the literature; (2) we determine the separation between types, and (3) we confirm the overall agreement in various parameter spaces. Figure 9 shows the distribution of detected periods and amplitudes. As reported by Oosterhoff (1939) and Silbermann & Smith (1995), we see a gap between the two main populations at a period value of  $\sim 0.5$  d.

Once the initial classification based on the main period is finished, we search for the secondary period to distinguish between RRC and RRd stars. We employ a modified non-linear discrete Fourier transform (DFT) method to construct an amplitude spectrum. The basic fitting method has been used in previous studies of multi-mode RR Lyrae stars, such as Gruberbauer et al. (2007):

$$\text{mag} = A_0 + \sum_i^{i_{\max}} A_i \cos(2\pi f_i t - \theta_i) . \quad (3)$$

In order to further improve the accuracy of this method, we minimize the template effect as discussed in previous sections by fitting a template-free function (i.e., with higher harmonics):

$$\text{mag} = A_0 + \sum_i^{i_{\max}} A_i \mathcal{F}_i(2\pi f_i t) , \quad (4)$$

where  $\mathcal{F}_i$  is the normalized best-fit Fourier series  $\mathcal{F}_i(f) =$

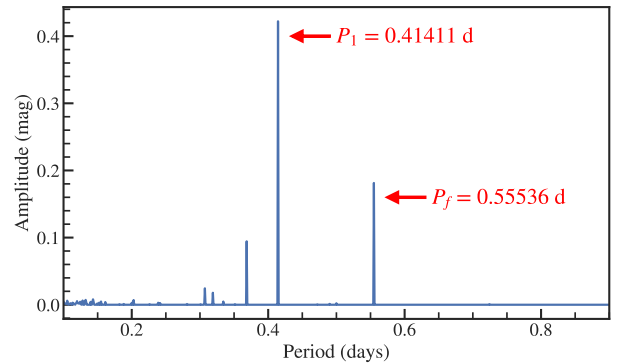


**Figure 8.** Amplitude Spectrum for V053 with our photometry data. The fundamental mode  $P_1$  and the secondary pulsation (fundamental) mode  $P_f$  can be clearly seen.

$\sum_k^{k_{\max}} a_k \cos(2\pi f k t) + b_k \sin(2\pi f k t)$ <sup>6</sup>. The frequency  $f_i$  at which the function is evaluated is determined by our main period-search method described in Sec. 3.1.2. This method is effective at detecting the pulsation modes in the resulting amplitude spectrum, since the harmonic components of the target frequencies at each pulsation mode are fitted (i.e., removed) at each iteration. Figure 8 is an example of our obtained amplitude spectra.

As our goal is to distinguish between RRC and RRd stars, this method can be further simplified to the analysis of the two strongest signals,  $i = 1, 2$ , for the first overtone and fundamental mode, respectively:

$$V = A_0 + A_1 \mathcal{F}_1\left(\frac{2\pi t}{P_1}\right) + A_f \mathcal{F}_f\left(\frac{2\pi t}{P_f}\right) \quad (5)$$

where  $\mathcal{F}_1$  is the normalized best-fit Fourier function to the first over-

<sup>6</sup> Equivalently,  $\mathcal{F}_i(f) = \sum_k^{k_{\max}} c_k \cos(2\pi f k t - \theta_k)$ .

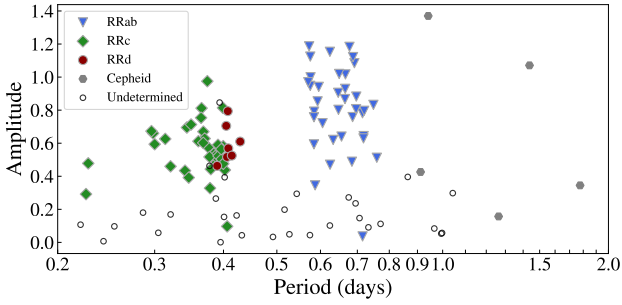


**Figure 9.** Classification based on the Bailey (period-amplitude) diagram. These data are used to make initial guesses for the dominant component in the double-mode analysis. RRd stars whose type is determined after double-mode analysis are overlaid.

tone at  $P_1$  and  $\mathcal{F}_f$  is the Fourier function fitted to the fundamental pulsation mode at  $P_f$ . The method of searching for the secondary period  $P_f$  is identical to searching for the main period as described in 3.1.2, except that the  $\chi^2$  value is evaluated against the residuals  $V_{\text{res},i} = y_i - A_1 \mathcal{F}_1 [(2\pi t_i)(P_1)]$  (‘prewhitened’ data, e.g. Blomme et al. 2011). This residual fitting is then further optimized with linear regression to fine-tune the value of  $P_f$ . This method is similar to that seen in e.g., Soszyński et al. (2009), Jurcsik et al. (2015), Moskalik & Poretti (2003).

We identify RRd stars by first selecting stars with  $0.7 < P_1/P_f < 0.8$  as suggested by (e.g. Jurcsik et al. 2015), and then evaluating the False Alarm Probability (FAP; for review, see VanderPlas 2018) of the detected secondary period in a Lomb-Scargle periodogram with a threshold of  $\text{FAP} < 0.001$ . This value is empirically determined to remove the most of the false secondary periods detected for RRab and RRc stars. The resulting periods and amplitudes signals are shown in Fig. 8. Using the two strongest signals, we can work to decouple the modes by subtracting each term  $\mathcal{F}_i$  from the raw data. The intermediate periodogram used to select a peak to evaluate the amplitude and resulting decoupled modes is shown in Fig. 7<sup>7</sup>, along with the resulting decoupled modes. To check this procedure against known data, we performed the same analysis on OGLE RRd stars (Soszyński et al. 2011). Our results are in a good agreement with the secondary period information provided by OGLE (for an example, see Fig. B9).

## 4 RESULTS

### 4.1 Period Determinations

We have determined periods and types for 79 variable stars, of which 74 were RR Lyrae stars and five were Type II Cepheid stars. The results of our analysis are presented in Table A1, which includes the ID, position, best-fit period determination and its uncertainty, amplitude, and type classification for each star we considered. The period error is determined by taking the largest uncertainties out of three sources: instrumental (lowest digit of the telescope timestamp), statistical (randomness in the fitting algorithm), and algorithmic (insufficient  $\chi^2$  search scaling) errors. We believe that the

<sup>7</sup> The increased noise floor and signal level is an expected behaviour for a periodogram with multi-term fitting. For review, see VanderPlas (2018).

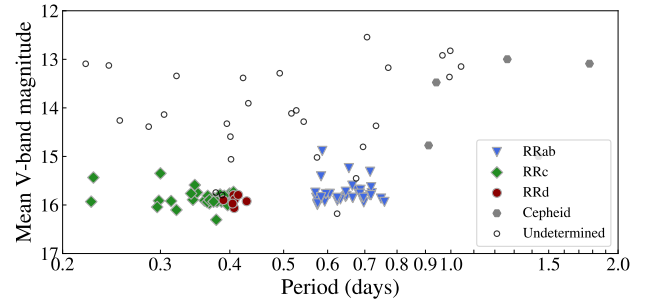


**Figure 10.** Mean V-band magnitude of star and main pulsation period of each star. Type II Cepheid variables are well isolated from RR Lyrae stars, and the brighter magnitude of undetermined stars suggests contamination from nearby stars.

resulting uncertainties ( $\sim 10^{-7}$  d) are more accurate and meaningful than many previously reported uncertainties, which are generally calculated by taking the instrumental timestamp uncertainty divided by the number of periods spanned during observations. We show our phase-folded light curves in Figures B1–B7, with the addition of two decomposed pulsation modes for double-mode RRd stars.

We compared our results to similar works in our references and found that there is general agreement between all works, although a small number of stars have classifications which vary between our references. Some of our results (e.g. V16, V35, V51, V93, V118) do not agree with the references, however, we note that our disagreement with the references is not more common than the disagreement between the references themselves.

### 4.2 Stars by Classification Type

Out of 79 total variable stars, we find 33 RRab stars, with an average period of 0.65 d. These stars are clearly distinguished by their sharply peaked maxima and are single-mode pulsators<sup>8</sup>. We classify 34 stars as RRc with an average period of 0.35 d, and with light curves showing near-sinusoidal shapes unique to first-overtone pulsation. We find 7 RRd multimode stars with an average period of 0.41 d, although we note that this period value is specific to the first overtone when considering multimode pulsators. With our double-mode analysis, we obtained mean value of  $A_f/A_1$  of 0.37 for RRd stars. While less common in M15, we also detect 5 Type II Cepheid variables, with an average period of 1.26 d. These Type II Cepheid light curves are similar to those of RRab stars, as they pulsate in the fundamental mode, but their forms vary and we do not perform a detailed analysis of them.

As shown by Catelan (2009), Mean RRab periods and minimum RRab periods serve as reliable indicators of Oosterhoff type. Our value,  $\langle P_{\text{ab}} \rangle = 0.65$  d and  $(P_{\text{ab}})_{\text{min}} = 0.57$  d suggests M15 is OoII type. This is consistent with previously reported results (e.g. Oosterhoff 1939 and Corwin et al. 2008).

We made 34 possible detections of variable stars, in addition to the 74 about which we are confident. This undetermined population typically belongs to the ‘‘large distance’’ group identified in Figure 2

<sup>8</sup> Note that these distinguishing features are not used for classification, but that the clear differences support classification via separation in period-amplitude space.

and are not firmly classified owing to possible contamination and a small SNR. Stars marked with “??” are undetermined.

The overall population distribution in the Bailey (period-amplitude) diagram (Fig. 9) shows some notable characteristics, such as (a) a short pulsation ( $\sim 0.2\text{--}0.4$  d) with a relatively small amplitude ( $\lesssim 0.9$  mag) for RRc stars, (b) a narrow period range for RRd stars ( $P \approx 0.39\text{--}0.43$  d), (c) no confirmed detections of variable stars with  $P \approx 0.5$  d, and (d) RRab stars having a wide range in amplitude (0.4–1.3 mag) but a small range in period ( $P \approx 0.55\text{--}0.75$  d). These characteristics are consistent with existing studies of M15 (e.g., Corwin et al. (2008), Silbermann & Smith (1995), Arellano Ferro et al. (2006)). We note that RR Lyrae populations not constrained by the narrow metallicity range of M15 will display more variation.

When our stars are plotted in period-magnitude space as seen in Figure 10, all types of RR Lyrae stars are tightly gathered at a similar apparent  $V$ -band magnitude of  $V \approx 16$  mag. This is consistent with previous observations (e.g., Bingham et al. 1984; Silbermann & Smith 1995), and clearly shows the separation of Type II Cepheid stars from RR Lyrae stars, which are brighter and have longer pulsation times. Our undetermined stars are often brighter, and there is no consistency in their measured periods, which span values belonging to all RR Lyrae types as well as Type II Cepheids. This suggests that the majority of the undetermined stars are contaminated by nearby objects, raising their perceived brightness but leaving a wide range of period values.

For stars with multi-mode pulsations, it is of interest to take the amplitude ratio of the fundamental mode,  $A_f$ , and the first overtone,  $A_1$ . In our sample of RRd stars we see a mean value of  $\langle A_f/A_1 \rangle \approx 0.371$  (with a standard deviation of  $\sigma_{A_f/A_1} \approx 0.065$ ), suggesting that this ratio is relatively consistent across our RRd stars. We note that our RRd stars have  $A_f/A_1$  values  $\leq 1$ , suggesting that the first overtone is slightly more dominant in these RRd stars. This is consistent with other observations, such as Jurcsik et al. (2015).

The ratio of the periods of the fundamental mode and the first overtone is also a notable feature of the multimode RRd stars. Prior work suggests that this ratio should be quite narrow (see Clementini et al. 2016), and our results support this with bounds of  $0.745 \leq P_1/P_f \leq 0.747$  and a mean  $\langle P_1/P_f \rangle = 0.746$ .

### 4.3 Notes on Individual Stars

**V027** – We confirm that V27 does not appear to be a variable star, as has been noticed since at least Sawyer Hogg (1973).

**V095** – This variable has a period of 1.263 d, and peaks brighter than 13 mag. No period determinations for this star can be found in the reference literature, likely owing to brightness contamination resulting from close proximity to the core of M15. The period and brightness of this star suggest that it is a Type II Cepheid variable.

**V107** – Both the light-curve shape and the period of 0.277 d suggest that it is an RRc star. No previous determinations for the period can be found in the reference literature.

**V123** – While the light-curve shape is unclear, the period of 0.715 d and the magnitude range suggest that this is an RRab star. No previous determinations for the period can be found in the reference literature.

**V140** – This variable peaks brighter than 13 mag and has a relatively long period of 1.776 d, suggesting that it is a Type II Cepheid

variable. No previous determinations for the period can be found in the reference literature.

**V155** – Another bright star with a long period of 0.912 d, this variable is also likely a Type II Cepheid, and does not have a previous period determination in the reference literature.

**Possible detections** – Of those variables without classifications, we have detected 10 objects with no previously reported periods in our references: V079, V106a, V106b, V110, V115, V121, V143, V147, V150, V154, and V158. V106a shows a large secondary period with a ratio of  $P_1/P_f \approx 0.75$ , suggesting it is a possible RRd star. These stars require further confirmation and investigation.

## 5 CONCLUSION AND FUTURE WORK

Using the Nickel telescope at Lick Observatory, we observed M15 over 46 nights and accumulated 691 images. In tandem, we have developed a custom pipeline to detect periodic behaviour in our data. We compared this new, purpose-built pipeline to existing techniques using the Gaia data release and found our results to be highly encouraging. We discussed the analysis of single and multimode pulsators, as well as the uncertainty treatment in our pipeline. Our analysis led to confident period classifications for 74 RR Lyrae stars in M15, two of which do not have a value listed in the reference literature. Of these 74 stars, the majority (67) are single-mode pulsators, which are classified as RRab and RRc stars.

Looking to the future, we note that the long-term period evolution of RR Lyrae stars is not well constrained by either theory or observation (Jurcsik & Hajdu 2017). The difficulty of making a sufficiently accurate period determination, combined with the long timescales required to see this change, restrict the effectiveness of observationally constraining this behaviour, and theoretical derivations remain challenging (Stellingwerf et al. 1987). Long-term, high-quality data are necessary for investigating the temporal evolution of RR Lyrae stars. With the addition of the results presented herein, we plan to conduct such an investigation in a subsequent paper (Murakami et al., in prep.).

## ACKNOWLEDGEMENTS

We acknowledge Josh Bloom and Dan Weisz for thought-provoking discussions of period analysis and validation, and Arjun Savel for providing knowledge on data-analysis tools. This research made use of Astropy,<sup>9</sup> a community-developed core Python package for astronomy (Astropy Collaboration et al. 2013; Price-Whelan et al. 2018). We acknowledge generous support from the TABASGO Foundation, Marc J. Staley, the Christopher R. Redlich Fund, and the Miller Institute for Basic Research in Science (U.C. Berkeley). Research at Lick Observatory is partially supported by a generous gift from Google. We also thank the student observers involved with the research group: Samantha Stegman, Julia Hestenes, Keto Zhang, Raphael Baer-Way, Teagan Chapman, Matt Chu, Asia de-Graw, Nachiket Girish, Romain Hardy, Connor Jennings, Evelyn Lu, Emily Ma, Emma McGinness, Shaunak Modak, Derek Perera, Druv Punjabi, Jackson Sipple, James Sunseri, Kevin Tang, Sergiy Vasylyev, Jeremy Wayland, and Abel Yagubyan. We also appreciate the assistance of the staff at Lick Observatory.

<sup>9</sup> <http://www.astropy.org>



## DATA AVAILABILITY

The raw photometry data used in our analysis is available at <https://github.com/SterlingYM/M15data2020>, and also upon request to an author.

## REFERENCES

- Arellano Ferro A., García Lugo G., Rosenzweig P., 2006, *Rev. Mex. Astron. Astrofis.*, **42**, 75
- Arellano Ferro A., Rosenzweig P., Luna A., Deras D., Muneer S., Giridhar S., Michel R., 2018, *Astronomische Nachrichten*, **339**, 158–167
- Astropy Collaboration et al., 2013, *A&A*, **558**, A33
- Bailey S. I., 1902, *Annals of Harvard College Observatory*, **38**, 1
- Bailey S. I., Leland E. F., Woods I. E., Pickering E. C., 1919, *Annals of Harvard College Observatory*, **78**, 195
- Benkő J. M., et al., 2010, *MNRAS*, **409**, 1585
- Bingham E. A., Cacciari C., Dickens R. J., Pecci F. F., 1984, *MNRAS*, **209**, 765
- Blažko S., 1907, *Astronomische Nachrichten*, **175**, 325
- Blomme R., et al., 2011, *A&A*, **533**, A4
- Budding E., Demircan O., 2007, *Introduction to Astronomical Photometry*. Cambridge Observing Handbooks for Research Astronomers Vol. 6, Cambridge University Press
- Catelan M., 2009, *Ap&SS*, **320**, 261
- Clement C. M., et al., 2001, *AJ*, **122**, 2587
- Clementini G., et al., 2016, *Astronomy & Astrophysics*, **595**, A133
- Corwin T. M., Borissova J., Stetson P. B., Catelan M., Smith H. A., Kurtev R., Stephens A. W., 2008, *The Astronomical Journal*, **135**, 1459
- Fadeyev Y. A., 2018, *Astronomy Letters*, **44**, 616
- Filippenko A. V., Simon R. S., 1981, *AJ*, **86**, 671
- Gruberbauer M., et al., 2007, *MNRAS*, **379**, 1498
- Holl B., et al., 2018, *A&A*, **618**, A30
- Jurcsik J., Hajdu G., 2017, *MNRAS*, **470**, 617
- Jurcsik J., Benk J. M., Bakos G. ., Szeidl B., Szab R., 2003, *The Astrophysical Journal*, **597**, L49–L52
- Jurcsik J., et al., 2006, *AJ*, **132**, 61
- Jurcsik J., et al., 2015, *ApJS*, **219**, 25
- Kolláth Z., Buchler J. R., Szabó R., Csabry Z., 2002, *A&A*, **385**, 932
- Kovács G., Kupi G., 2007, *A&A*, **462**, 1007
- Landolt A. U., 1983, *AJ*, **88**, 439
- Landolt A. U., 1992, *AJ*, **104**, 340
- Lomb N. R., 1976, *Ap&SS*, **39**, 447
- Makarova V. A., Akimova V. P., 1965, *Peremennye Zvezdy*, **15**, 350
- Mannino G., 1956, *Mem. Soc. Astron. Italiana*, **27**, 169
- Mészáros S., et al., 2020, *MNRAS*, **492**, 1641
- Moskalik P., Poretti E., 2003, *A&A*, **398**, 213
- Oosterhoff P. T., 1939, *The Observatory*, **62**, 104
- Percy J. R., 2007, *Understanding Variable Stars*. Cambridge University Press
- Pickering E. C., Colson H. R., Fleming W. P., Wells L. D., 1901, *ApJ*, **13**, 226
- Pietrukowicz P., et al., 2020, arXiv e-prints, p. arXiv:2007.05849
- Price-Whelan A. M., et al., 2018, *AJ*, **156**, 123
- Prudil Z., Skarka M., 2017, *Monthly Notices of the Royal Astronomical Society*, **466**, 2602
- Samus' N. N., Kazarovets E. V., Durlevich O. V., Kireeva N. N., Pastukhova E. N., 2017, *Astronomy Reports*, **61**, 80
- Sarajedini A., et al., 2019, *VizieR Online Data Catalog*, p. J/AJ/133/1658
- Sawyer Hogg H., 1973, *Publications of the David Dunlap Observatory*, **3**, 6
- Scargle J. D., 1982, *ApJ*, **263**, 835
- Scolnic D., et al., 2019, *Astro2020: Decadal Survey on Astronomy and Astrophysics*, **2020**, 270
- Siegel M. H., Porterfield B. L., Balzer B. G., Hagen L. M. Z., 2015, *AJ*, **150**, 129
- Silbermann N. A., Smith H. A., 1995, *AJ*, **110**, 704
- Smolec R., 2016, arXiv preprint arXiv:1603.01252
- Smolec R., Moskalik P., 2012, *MNRAS*, **426**, 108
- Soszyński I., et al., 2009, *Acta Astron.*, **59**, 1
- Soszyński I., et al., 2011, *Acta Astron.*, **61**, 1
- Stahl B. E., et al., 2019, *Monthly Notices of the Royal Astronomical Society*, **490**, 3882–3907
- Stellingwerf R. F., 1975, *ApJ*, **199**, 705
- Stellingwerf R. F., Gautschy A., Dickens R. J., 1987, *ApJ*, **313**, L75
- Szabó R., et al., 2014, *Astronomy & Astrophysics*, **570**, A100
- Tonry J. L., et al., 2012, *ApJ*, **750**, 99
- VanderPlas J. T., 2018, *The Astrophysical Journal Supplement Series*, **236**, 16
- Virtanen P., et al., 2020, *Nature Methods*, **17**, 261
- Wemple L., 1932, *Harvard College Observatory Bulletin*, **889**, 9

## APPENDIX A: TABLE

Table A1: Results.

ID	$\alpha$ (J2000) (deg)	$\delta$ (J2000) (deg)	$P$ (days)	$\sigma_P$ (days)	$P_2$ (days)	$\sigma_{P_2}$ (days)	$A_1$ (mag)	$A_2$ (mag)	$\bar{V}$ (mag)	Type
V001	322.4590	12.1740	1.437837434	3.7e-07	-	-	1.07	-	14.99	CephII
V002	322.4438	12.1687	0.684304375	1.6e-07	-	-	0.49	-	15.74	RRab
V003	322.4222	12.1539	0.388720632	8.5e-06	-	-	0.48	-	15.83	RRc
V004	322.4610	12.1216	0.313589117	2.4e-08	-	-	0.63	-	15.92	RRc
V005	322.4646	12.1081	0.384211954	7.2e-08	-	-	0.54	-	15.78	RRc
V006	322.4995	12.1886	0.666015094	1.7e-07	-	-	1.02	-	15.86	RRab
V007	322.4955	12.1879	0.367563437	1.2e-06	-	-	0.63	-	15.97	RRc
V008	322.4924	12.2027	0.646238777	3.9e-06	-	-	0.91	-	15.84	RRab
V009	322.4967	12.2059	0.715282097	5.7e-07	-	-	0.78	-	15.80	RRab
V010	322.5284	12.1680	0.386389721	2.1e-06	-	-	0.52	-	15.93	RRc
V011	322.5416	12.1617	0.343265510	5.5e-08	-	-	0.69	-	15.89	RRc
V012	322.5387	12.1535	0.592875644	5.2e-07	-	-	0.85	-	15.93	RRab
V013	322.5288	12.1485	0.574910937	1.4e-07	-	-	0.95	-	15.98	RRab
V015	322.5164	12.0831	0.584394482	1.6e-07	-	-	0.79	-	15.86	RRab
V016	322.5210	12.2035	0.399195555	3.3e-07	-	-	0.81	-	15.84	RRc
V017	322.5163	12.1981	0.428912296	1.5e-07	0.575678	1.3e-05	0.61	0.20	15.92	RRd
V018	322.5145	12.1954	0.367725969	1.0e-07	-	-	0.67	-	15.87	RRc
V019	322.5240	12.2121	0.572306432	1.9e-06	-	-	1.19	-	15.85	RRab
V020	322.5156	12.1648	0.696958720	4.3e-07	-	-	0.88	-	15.95	RRab
V021	322.5023	12.1513	0.648795261	3.6e-06	-	-	1.02	-	15.82	RRab
V022	322.3988	12.1539	0.720230076	1.6e-06	-	-	0.80	-	15.76	RRab
V023	322.5466	12.2388	0.632698496	1.6e-07	-	-	0.62	-	15.89	RRab
V024	322.4624	12.1654	0.369691742	1.1e-07	-	-	0.63	-	15.87	RRc
V025	322.5786	12.1650	0.665318041	6.2e-06	-	-	0.93	-	15.85	RRab
V026	322.4986	12.2595	0.402317102	4.4e-08	-	-	0.44	-	15.94	RRc
V029	322.5385	12.2263	0.575015865	1.5e-05	-	-	1.12	-	16.00	RRab
V030	322.4458	12.1661	0.405998183	8.0e-08	0.544739	1.3e-05	0.52	0.19	15.80	RRd
V031	322.4602	12.2352	0.408183108	6.0e-08	0.547051	1.9e-05	0.57	0.21	15.88	RRd
V032	322.4781	12.1972	0.605303420	1.3e-07	-	-	0.72	-	15.77	RRab
V033	322.4812	12.1593	0.583940164	3.5e-08	-	-	0.76	-	15.41	RRab
V034	322.4771	12.1521	0.400960355	-	-	-	0.15	-	-	??
V035	322.4834	12.1219	0.624546598	2.6e-07	-	-	0.47	-	15.91	RRab
V036	322.4850	12.1447	0.624130821	2.2e-06	-	-	1.15	-	15.85	RRab
V038	322.4950	12.1268	0.375280597	4.2e-08	-	-	0.57	-	15.87	RRc
V039	322.4986	12.1328	0.389551691	5.2e-08	0.522278	1.2e-05	0.46	0.16	15.90	RRd
V040	322.5301	12.1351	0.377331483	4.1e-08	-	-	0.52	-	15.92	RRc
V041	322.5107	12.1521	0.391761515	2.5e-06	-	-	0.52	-	15.88	RRc
V042	322.5575	12.1575	0.360188851	5.2e-08	-	-	0.61	-	15.91	RRc
V044	322.5185	12.1685	0.595669649	4.8e-06	-	-	0.94	-	15.77	RRab
V045	322.5116	12.1588	0.677404150	1.9e-06	-	-	1.18	-	15.69	RRab
V046	322.5090	12.1764	0.691443810	3.6e-06	-	-	1.08	-	15.84	RRab
V047	322.5052	12.1664	0.687547509	1.4e-06	-	-	1.12	-	15.69	RRab
V048	322.5093	12.2092	0.364972072	7.2e-08	-	-	0.81	-	15.81	RRc
V049	322.5038	12.2136	0.655186807	4.3e-06	-	-	0.64	-	15.24	RRab
V050	322.5391	12.1954	0.298060627	4.6e-08	-	-	0.66	-	15.91	RRc
V051	322.4942	12.1928	0.396962319	1.3e-07	-	-	0.50	-	15.93	RRc
V052	322.5473	12.1616	0.575654124	3.6e-06	-	-	1.00	-	15.97	RRab
V053	322.4667	12.1365	0.414109598	9.3e-08	0.555360	1.4e-05	0.52	0.18	15.79	RRd
V054	322.4956	12.1919	0.399572367	6.1e-08	-	-	0.58	-	15.95	RRc
V055	322.5114	12.1622	0.748671788	3.9e-07	-	-	0.83	-	15.87	RRab
V056	322.5089	12.1676	0.570260593	1.7e-07	-	-	0.97	-	15.75	RRab
V057	322.5141	12.1522	0.349277148	5.6e-08	-	-	0.71	-	15.74	RRc
V058	322.4770	12.1697	0.407285449	9.1e-08	0.545823	1.1e-05	0.79	0.41	16.06	RRd
V059	322.5040	12.1769	0.431889913	-	-	-	0.04	-	-	??
V060	322.5080	12.1510	0.718689553	3.6e-07	-	-	0.64	-	15.63	RRab

Continued on next page

Table A1 – continued from previous page

ID	$\alpha$ (J2000) (deg)	$\delta$ (J2000) (deg)	$P$ (days)	$\sigma_P$ (days)	$P_2$ (days)	$\sigma_{P_2}$ (days)	$A_1$ (mag)	$A_2$ (mag)	$\bar{V}$ (mag)	Type
V061	322.4737	12.1558	0.399688532	9.9e-08	-	-	0.48	-	15.77	RRc
V062	322.4724	12.1780	0.377318789	-	-	-	0.46	-	-	??
V063	322.5064	12.1760	0.646891427	1.4e-07	-	-	0.80	-	15.73	RRab
V064	322.4795	12.1728	0.364249404	1.2e-07	-	-	0.75	-	15.94	RRc
V065	322.4637	12.1566	0.718199490	4.5e-06	-	-	0.63	-	15.80	RRab
V066	322.4735	12.1362	0.379343054	3.7e-08	-	-	0.44	-	15.93	RRc
V067	322.4682	12.1644	0.404610074	1.2e-07	0.542406	1.0e-05	0.71	0.24	15.97	RRd
V068	322.4830	12.1703	0.387438607	-	-	-	0.26	-	-	??
V069	322.4822	12.1607	0.586772955	3.0e-07	-	-	0.35	-	14.89	RRab
V070	322.4831	12.1620	0.367582599	7.4e-08	-	-	0.60	-	15.90	RRc
V071	322.4827	12.1631	0.105774416	-	-	-	0.14	-	-	??
V072	322.4923	12.1769	0.686283385	2.8e-07	-	-	0.76	-	15.77	RRab
V073	322.4907	12.1724	0.401962763	-	-	-	0.39	-	-	??
V074	322.5035	12.1436	0.296010243	4.6e-08	-	-	0.67	-	16.04	RRc
V075	322.4927	12.1578	0.526924552	-	-	-	0.05	-	-	??
V076	322.4926	12.1610	0.320665464	-	-	-	0.17	-	-	??
V077	322.4898	12.1621	0.706426874	-	-	-	0.15	-	-	??
V078	322.4906	12.1806	0.664751545	1.9e-07	-	-	0.87	-	15.60	RRab
V079	322.4986	12.1611	0.285756395	-	-	-	0.18	-	-	??
V081	322.4877	12.1650	0.253480390	-	-	-	0.10	-	-	??
V082	322.4879	12.1678	0.491929862	-	-	-	0.03	-	-	??
V083	322.4982	12.1661	0.516328627	-	-	-	0.20	-	-	??
V084	322.4996	12.1634	0.543305073	-	-	-	0.29	-	-	??
V086	322.4964	12.1686	0.941440619	5.5e-07	-	-	1.37	-	13.48	CephII
V087	322.5010	12.1613	0.771371647	-	-	-	0.11	-	-	??
V089	322.4851	12.1666	0.304592260	-	-	-	0.06	-	-	??
V090	322.5025	12.1682	0.151975380	-	-	-	0.68	-	-	??
V091	322.5110	12.1753	0.390929100	1.2e-07	-	-	0.59	-	15.81	RRc
V092	322.4957	12.1603	0.373886851	8.7e-08	-	-	0.97	-	15.93	RRc
V093	322.5003	12.1587	0.340598884	6.8e-08	-	-	0.43	-	15.76	RRc
V094	322.4946	12.1750	0.395125307	-	-	-	0.00	-	-	??
V095	322.4939	12.1559	1.263577492	8.5e-07	-	-	0.16	-	13.00	CephII
V096	322.5393	12.2273	0.396360363	9.5e-08	-	-	0.56	-	16.00	RRc
V097	322.4701	12.1753	0.696354571	9.1e-07	-	-	0.81	-	15.85	RRab
V098	322.4735	12.1800	0.624063736	-	-	-	0.10	-	-	??
V099	322.5013	12.2209	0.225141886	4.6e-08	-	-	0.29	-	15.93	RRc
V100	322.4969	12.1566	0.320595991	8.0e-08	-	-	0.46	-	16.10	RRc
V102	322.5129	12.1755	0.759381107	1.9e-06	-	-	0.51	-	15.94	RRab
V103	322.4217	12.0908	0.583845056	1.4e-06	-	-	0.59	-	15.84	RRab
V106a	322.4846	12.1701	0.393562714	-	-	-	0.85	-	-	??
V106b	322.4840	12.1716	0.997568069	-	-	-	0.06	-	-	??
V107	322.4842	12.1604	0.227240473	3.5e-08	-	-	0.48	-	15.43	RRc
V110	322.5022	12.1562	0.675195633	-	-	-	0.27	-	-	??
V111	322.5048	12.1674	0.378130163	7.5e-08	-	-	0.33	-	16.30	RRc
V113	322.4947	12.0980	0.406180567	8.3e-08	-	-	0.10	-	15.73	RRc
V114	322.4935	12.1777	0.345933528	9.3e-08	-	-	0.39	-	15.59	RRc
V115	322.4962	12.1647	2.712286292	-	-	-	0.21	-	-	??
V116	322.4970	12.1532	0.965689926	-	-	-	0.08	-	-	??
V117	322.4992	12.1571	0.994196708	-	-	-	0.05	-	-	??
V118	322.4981	12.1821	0.299995772	7.8e-08	-	-	0.59	-	15.35	RRc
V119	322.4975	12.1697	0.733184352	-	-	-	0.09	-	-	??
V121	322.4840	12.2093	0.242234009	-	-	-	0.01	-	-	??
V122	322.5660	12.1741	0.574149201	-	-	-	0.04	-	-	??
V123	322.4289	12.1648	0.715498035	4.3e-06	-	-	0.04	-	15.32	RRab
V129	322.4922	12.1629	0.220068365	-	-	-	0.11	-	-	??
V140	322.4943	12.1673	1.776476681	1.1e-06	-	-	0.35	-	13.09	CephII
V143	322.4946	12.1612	0.694855607	-	-	-	0.24	-	-	??
V145	322.4973	12.1674	0.422570740	-	-	-	0.16	-	-	??

Continued on next page

Table A1 – continued from previous page

ID	$\alpha$ (J2000) (deg)	$\delta$ (J2000) (deg)	$P$ (days)	$\sigma_P$ (days)	$P_2$ (days)	$\sigma_{P_2}$ (days)	$A_1$ (mag)	$A_2$ (mag)	$\bar{V}$ (mag)	Type
V147	322.4958	12.1657	3.072484243	-	-	-	0.11	-	-	??
V150	322.4950	12.1715	1.043200501	-	-	-	0.30	-	-	??
V154	322.4916	12.1708	0.864274136	-	-	-	0.40	-	-	??
V155	322.4907	12.1697	0.911891427	2.7e-07	-	-	0.43	-	14.77	CephII
V158	322.4676	12.1031	0.118082890	-	-	-	0.68	-	-	??

Table A2: Calibration stars used with LPP\*.

#	Field	$\alpha_{\text{obs}}$ (deg)	$\delta_{\text{obs}}$ (deg)	$\alpha_{\text{diff}}$ (deg)	$\delta_{\text{diff}}$ (deg)	$V_{\text{cal}}$ (mag)	$V_{\text{obs}}$ (mag)	$V_{\text{diff}}$ (mag)	$\sigma V_{\text{obs}}$ (mag)
0	M15_1	322.519265	12.127833	0.000105	0.000066	15.273728	15.287983	0.014255	0.014855
1	M15_1	322.561284	12.140017	0.000107	0.000079	15.464006	15.442372	-0.021634	0.012730
2	M15_1	322.523107	12.118028	0.000107	0.000066	15.506678	15.530928	0.024250	0.012090
3	M15_1	322.533446	12.085643	0.000082	0.000070	15.992274	15.963761	-0.028513	0.013641
4	M15_1	322.543151	12.125756	0.000090	0.000072	15.990031	15.979094	-0.010937	0.014745
5	M15_1	322.534900	12.136032	0.000092	0.000070	16.048878	16.052094	0.003216	0.013421
6	M15_1	322.530015	12.109165	0.000103	0.000065	16.478746	16.496761	0.018014	0.019075
7	M15_1	322.554640	12.141452	0.000097	0.000077	16.790747	16.790150	-0.000597	0.020650
8	M15_1	322.567823	12.134789	0.000100	0.000079	17.252762	17.252872	0.000110	0.031925
9	M15_2	322.459429	12.150704	0.000109	0.000056	14.273025	14.260324	-0.012701	0.013764
10	M15_2	322.458902	12.159175	0.000105	0.000055	14.919133	14.922602	0.003468	0.010524
11	M15_2	322.445463	12.140651	0.000109	0.000055	14.930785	14.917324	-0.013461	0.009058
12	M15_2	322.456988	12.156429	0.000100	0.000061	15.089972	15.072546	-0.017426	0.015132
13	M15_2	322.458802	12.131101	0.000093	0.000046	15.189565	15.185824	-0.003741	0.016033
14	M15_2	322.447355	12.151231	0.000096	0.000063	15.412107	15.412935	0.000828	0.010156
15	M15_2	322.451633	12.155373	0.000094	0.000066	15.419053	15.430990	0.011937	0.022853
16	M15_2	322.462334	12.144905	0.000083	0.000051	15.454053	15.469824	0.015771	0.030308
17	M15_2	322.455935	12.140771	0.000115	0.000051	15.496215	15.507713	0.011498	0.018345
18	M15_3	322.521463	12.222239	0.000095	0.000064	14.395865	14.393613	-0.002252	0.014736
19	M15_3	322.519897	12.196303	0.000098	0.000067	14.553714	14.588363	0.034649	0.014014
20	M15_3	322.543955	12.236424	0.000120	0.000077	15.516245	15.496363	-0.019882	0.026960
21	M15_3	322.548378	12.234880	0.000116	0.000082	15.678872	15.663113	-0.015759	0.034030
22	M15_3	322.521121	12.227391	0.000099	0.000068	15.904249	15.909863	0.005614	0.014118
23	M15_3	322.533092	12.203466	0.000118	0.000068	15.965824	15.989238	0.023414	0.027297
24	M15_3	322.536526	12.208844	0.000107	0.000068	15.991126	15.992488	0.001362	0.021195
25	M15_3	322.540593	12.240000	0.000117	0.000073	16.044006	16.013488	-0.030518	0.022373
26	M15_4	322.448676	12.204609	0.000102	0.000045	14.526760	14.510128	-0.016632	0.015407
27	M15_4	322.448944	12.191813	0.000106	0.000057	15.115295	15.136328	0.021032	0.014781
28	M15_4	322.445159	12.195775	0.000119	0.000055	15.254565	15.249278	-0.005288	0.014280
29	M15_4	322.457367	12.208246	0.000083	0.000051	15.447569	15.461878	0.014309	0.013821
30	M15_4	322.435704	12.192173	0.000132	0.000054	15.380196	15.364628	-0.015568	0.023735
31	M15_4	322.464925	12.212959	0.000096	0.000056	15.770203	15.753778	-0.016425	0.020545
32	M15_4	322.469867	12.195119	0.000086	0.000062	15.896890	15.904128	0.007238	0.024449
33	M15_4	322.437433	12.198128	0.000116	0.000048	16.264444	16.270178	0.005733	0.024551
34	M15_4	322.456705	12.210754	0.000098	0.000048	15.987055	15.979578	-0.007477	0.018576
35	M15_4	322.457820	12.194107	0.000090	0.000065	16.547810	16.548878	0.001068	0.022561

\*The magnitude values are all in the V band.

“diff” is the deviation of the observed value (“obs”) from PS1 data (“cal”).



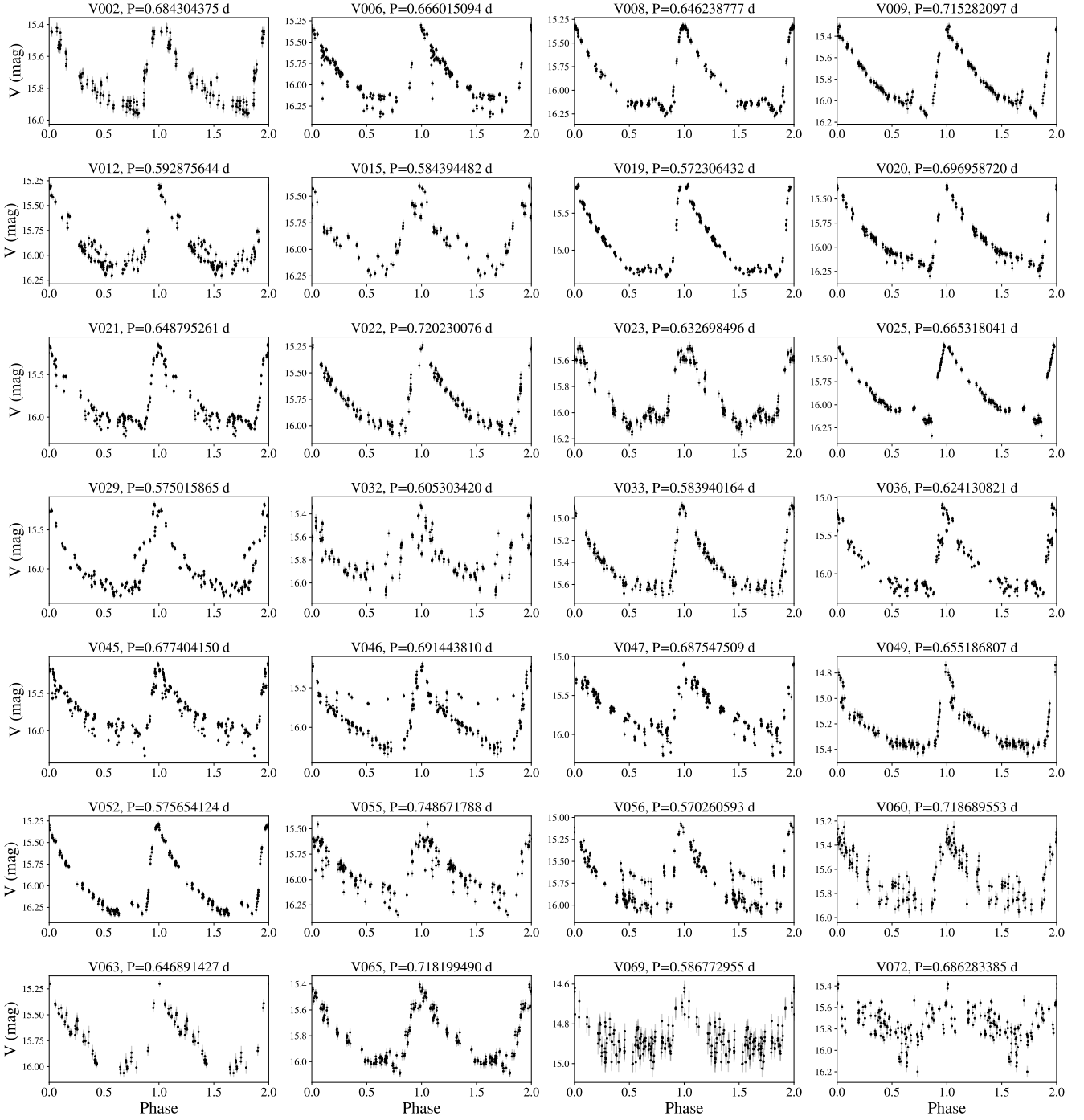


**Figure B1.** RRab stars: each cell is a folded light curve of a single-mode star pulsating in the fundamental mode (RRab). The abscissa is phase (normalised to a single period and repeated twice), and the ordinate is observed V -band magnitude.

## APPENDIX B: LIGHTCURVES

This paper has been typeset from a  $\text{\TeX}/\text{\LaTeX}$  file prepared by the author.

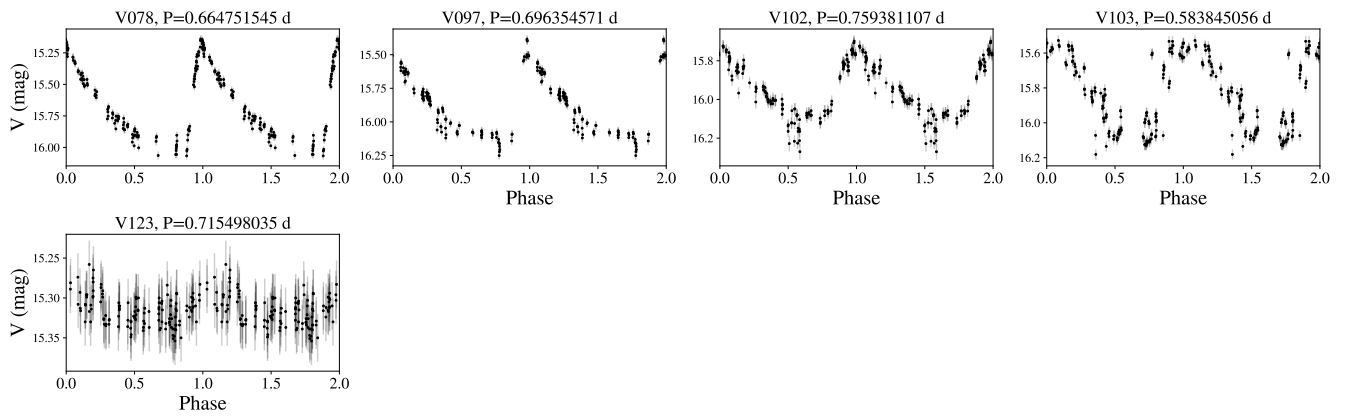


**Figure B2.** RRab stars (continued).

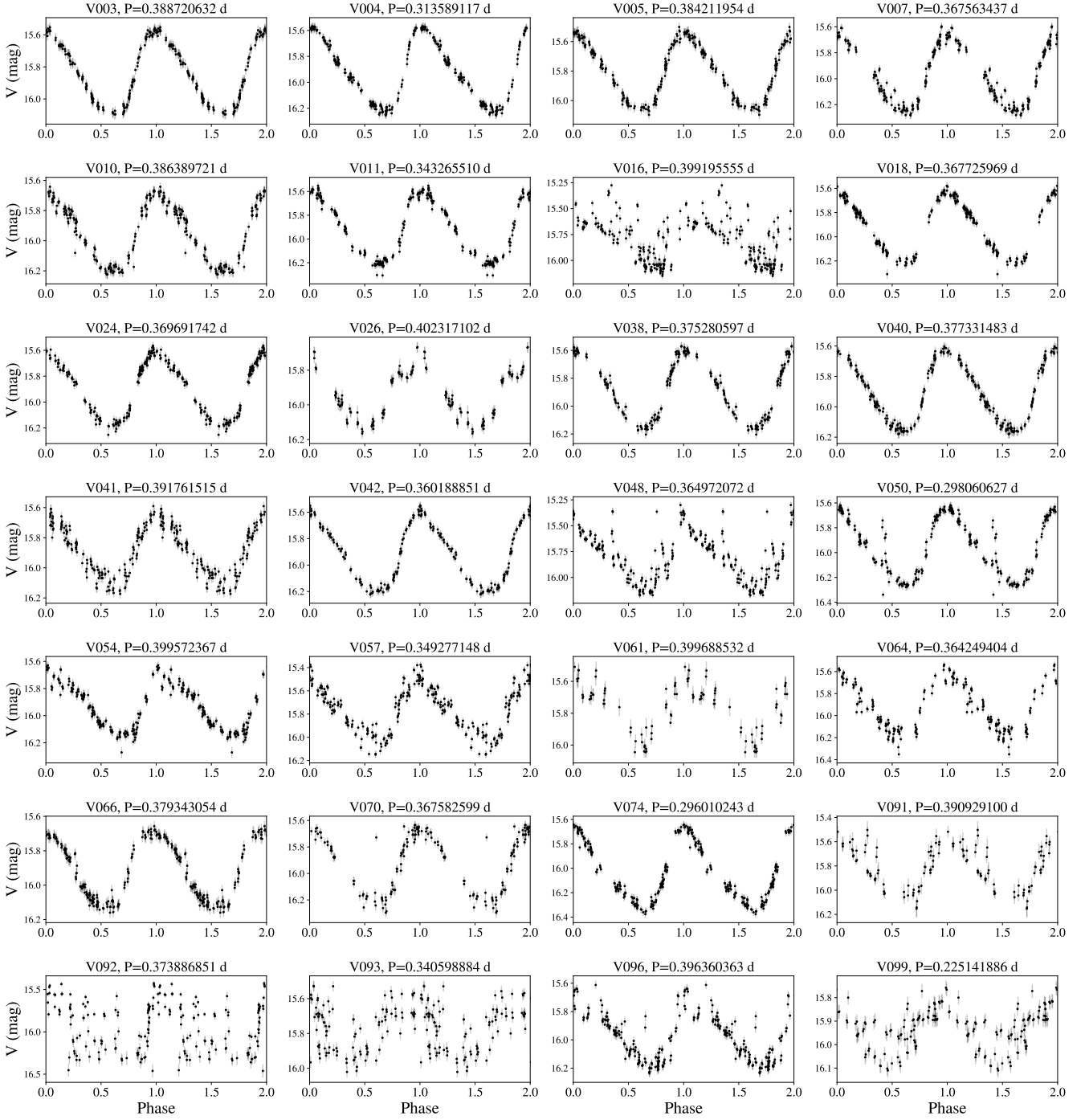


**Figure B3.** RRc stars. Conventions are the same as in Figure B1.

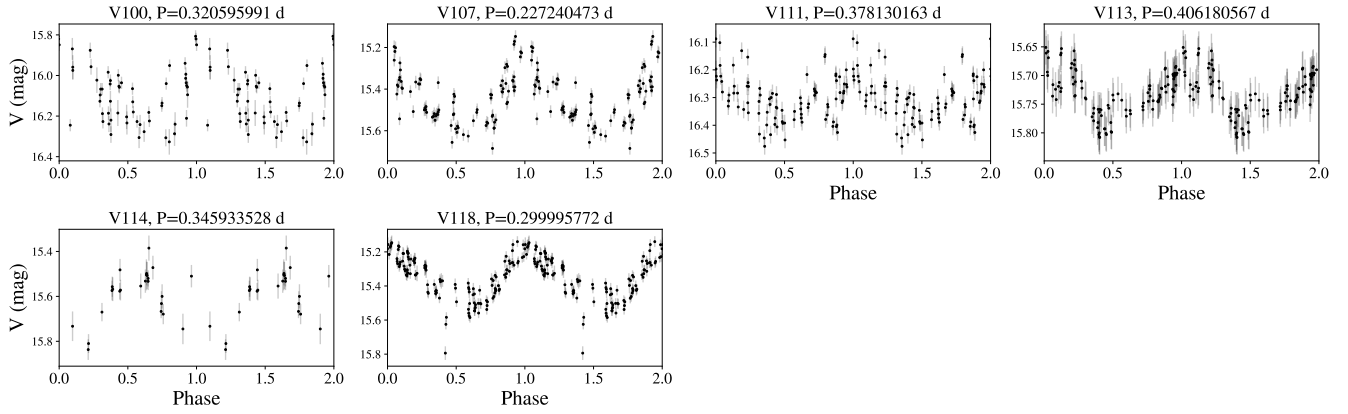


**Figure B4.** RRc stars (continued).

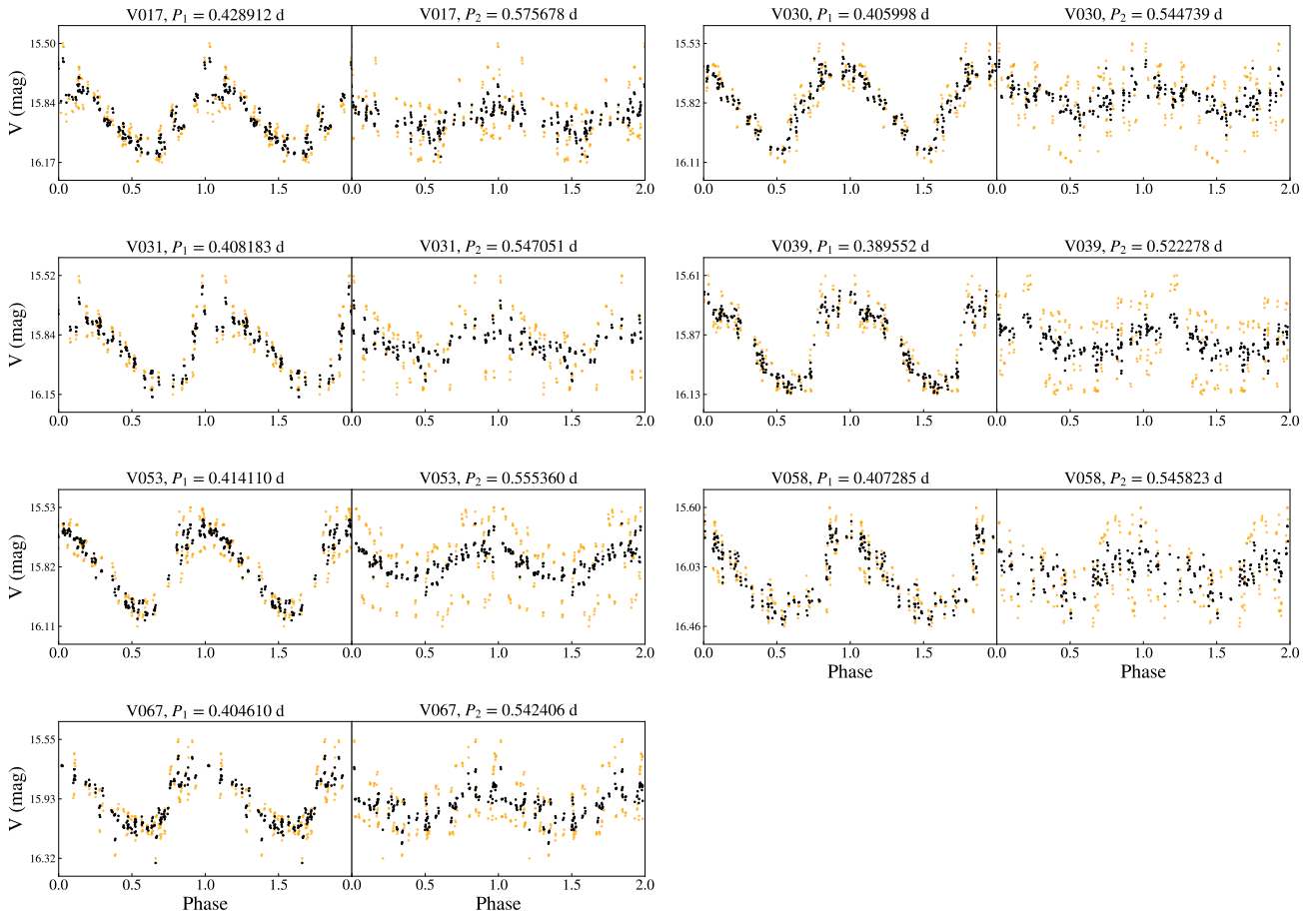


**Figure B5.** RRd stars: each set of plots represents a star pulsating in two periods simultaneously (RRd). Left columns show raw (yellow, thin color) and decoupled (black) data folded at the first overtone period ( $P_1$ ). Similarly, right columns show raw and decoupled data folded at the fundamental mode ( $P_f$ ).



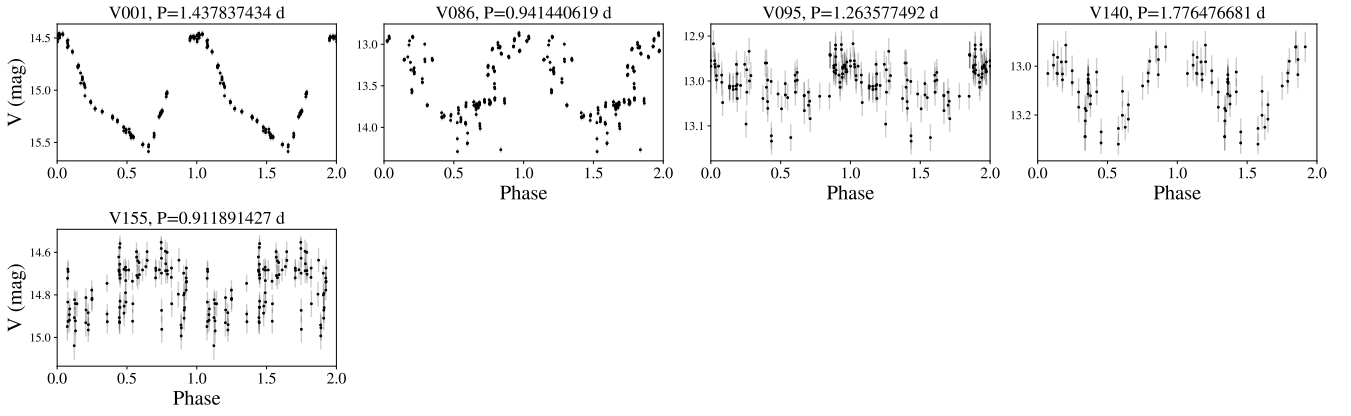


**Figure B6.** Type II Cepheid stars: each cell is a folded light curve of a single-mode star pulsating in the fundamental mode. While these stars exhibit morphological characteristics similar to those of RRab stars, these stars are brighter and have larger period values. The abscissa is phase (normalised to a single period and repeated twice), and the ordinate is observed V-band magnitude.

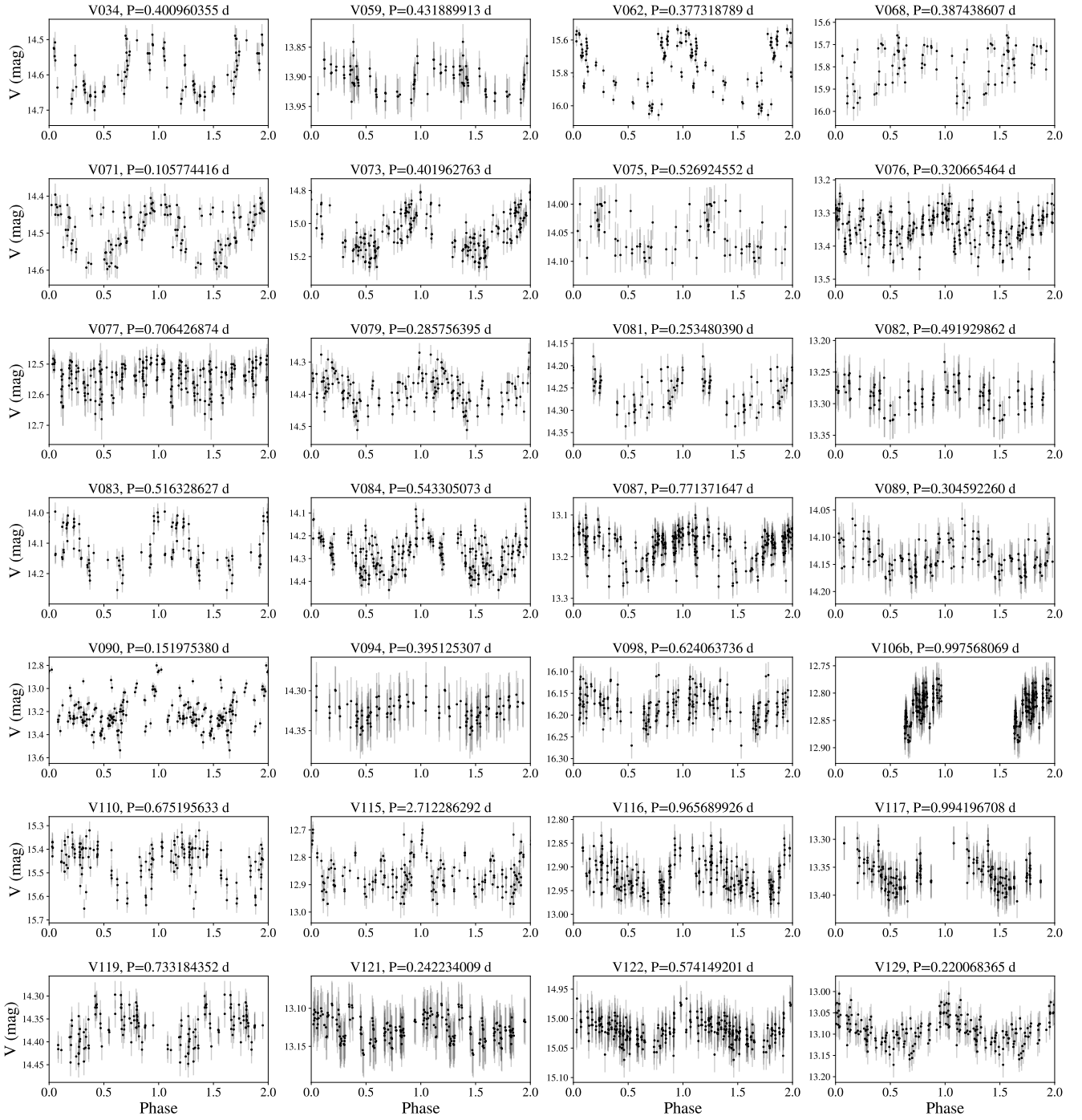


**Figure B7.** Stars with possible contamination (“undetermined” stars). Some of our detections had relatively large distances from known coordinates. This resulted in possible contamination by nearby stars and small SNR with relatively large intrinsic scatter. These stars are treated as questionable, and are not processed for type classification, although some light curves indicate that they may be RRc stars and main period. RRab stars and short-period Type II Cepheid stars cannot be distinguished owing to their common pulsation mode and inaccurate apparent magnitude. Since many of these stars do not have previously reported period values, we suggest our period estimation here.

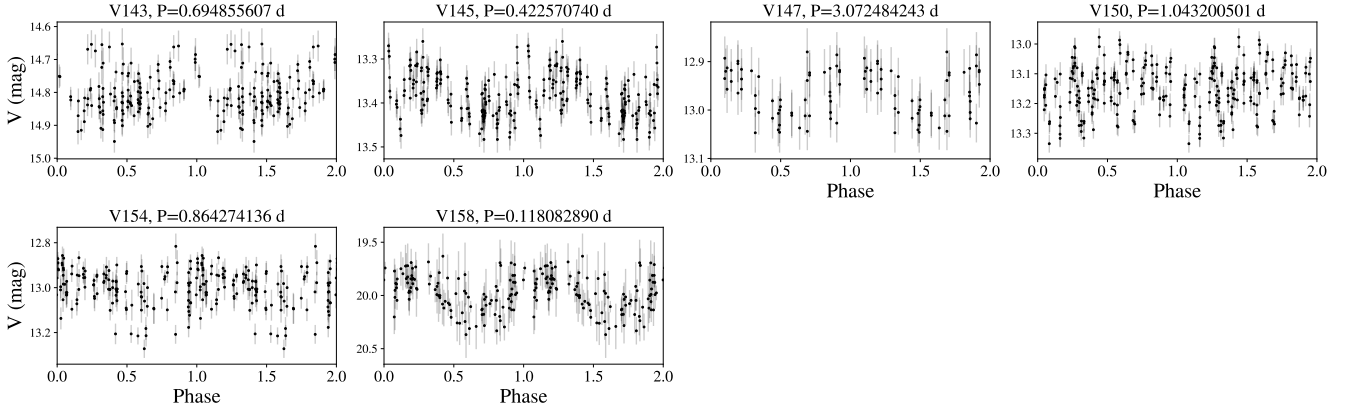


**Figure B8.** Stars with possible contamination (“undetermined” stars, continued).

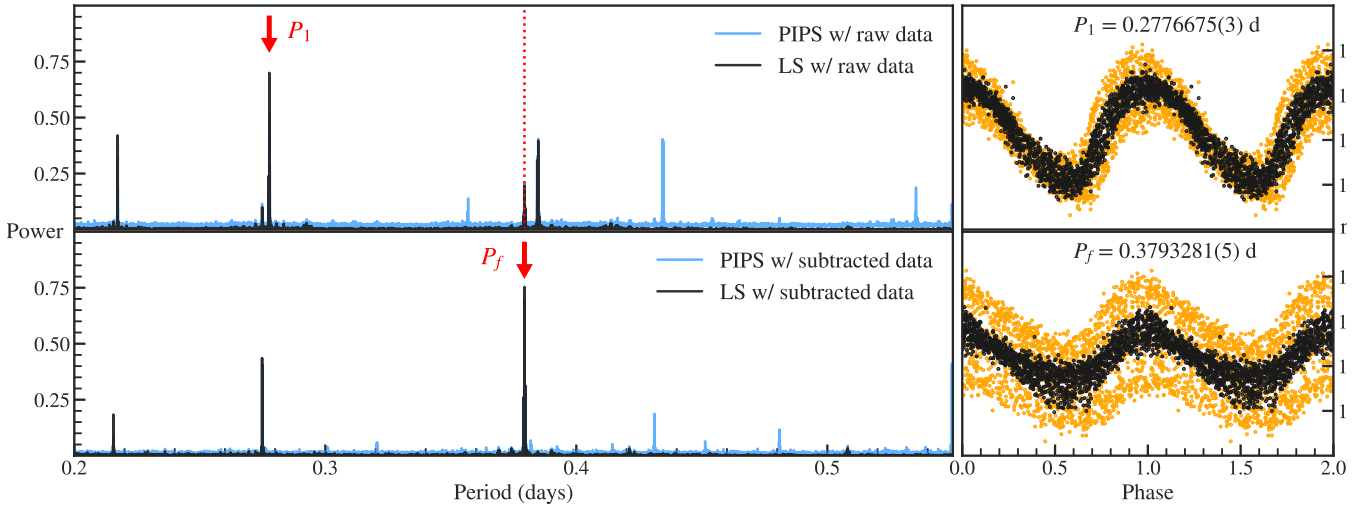


**Figure B9.** Same as Fig. 7, but for an RRd star reported by OGLE-III (OGLE-BLG-RRLYR-09258; Soszyński et al. 2011) as an example to validate our method. Our detection of both periods is in *perfect* agreement with the reported values by OGLE,  $P_{1,\text{OGLE}} = 0.2776675(1)$  and  $P_{f,\text{OGLE}} = 0.3793281(3)$ .

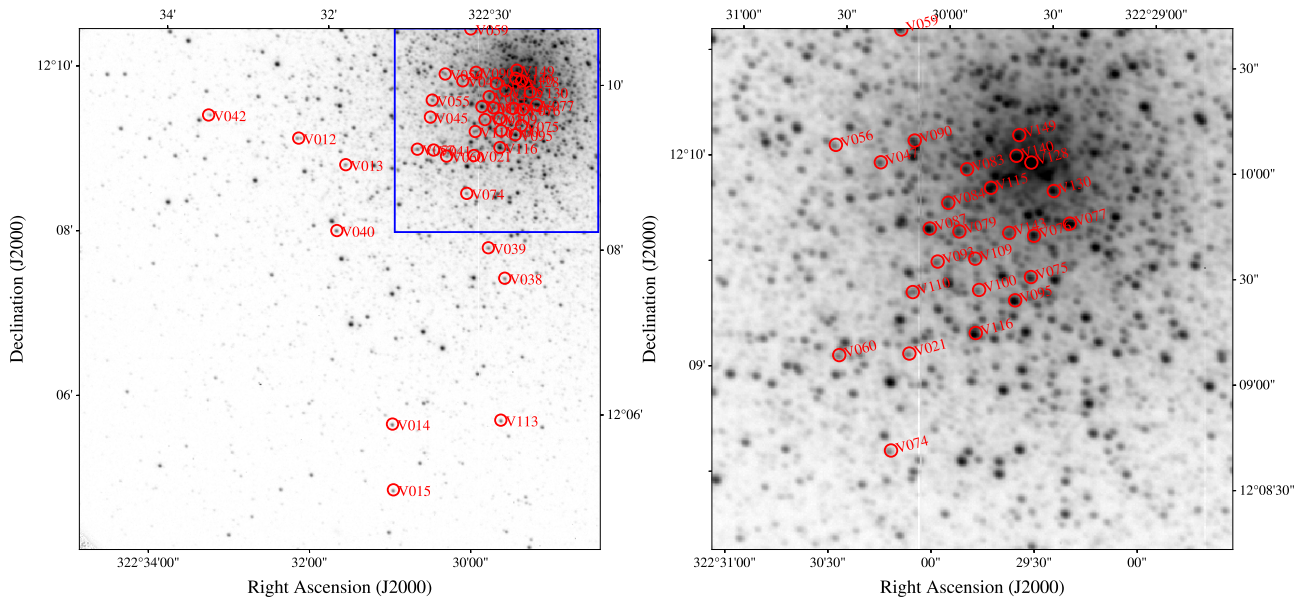


**Figure B10.** Left: *V* band image of the field M15\_1 and stars whose data from this field is used for our final results. Blue rectangle indicates the area shown in the right. Right: A close-up image near the centre.

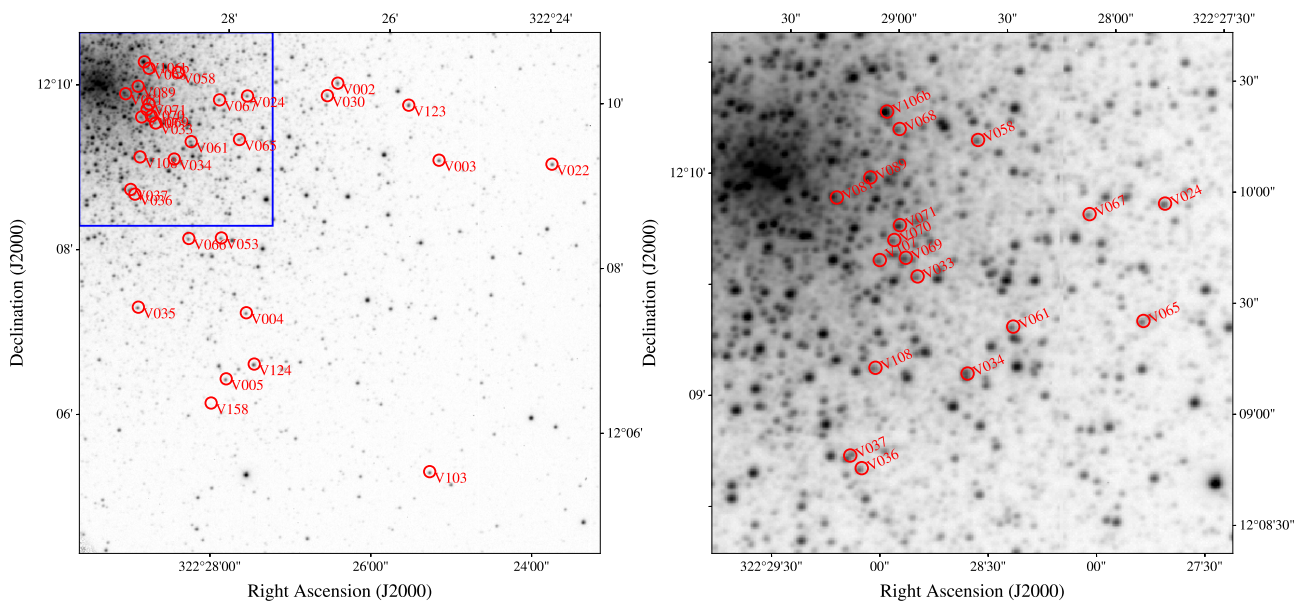


**Figure B11.** Field M15\_2. Conventions are the same as in Figure B10.



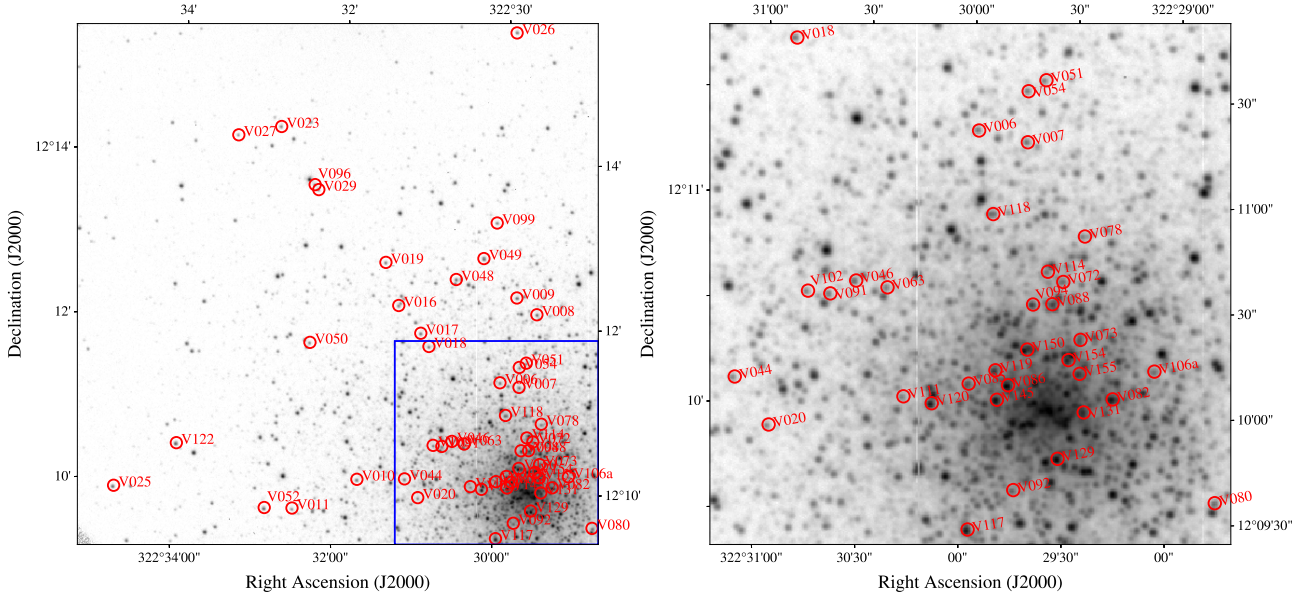


**Figure B12.** Field M15\_3. Conventions are the same as in Figure B10.

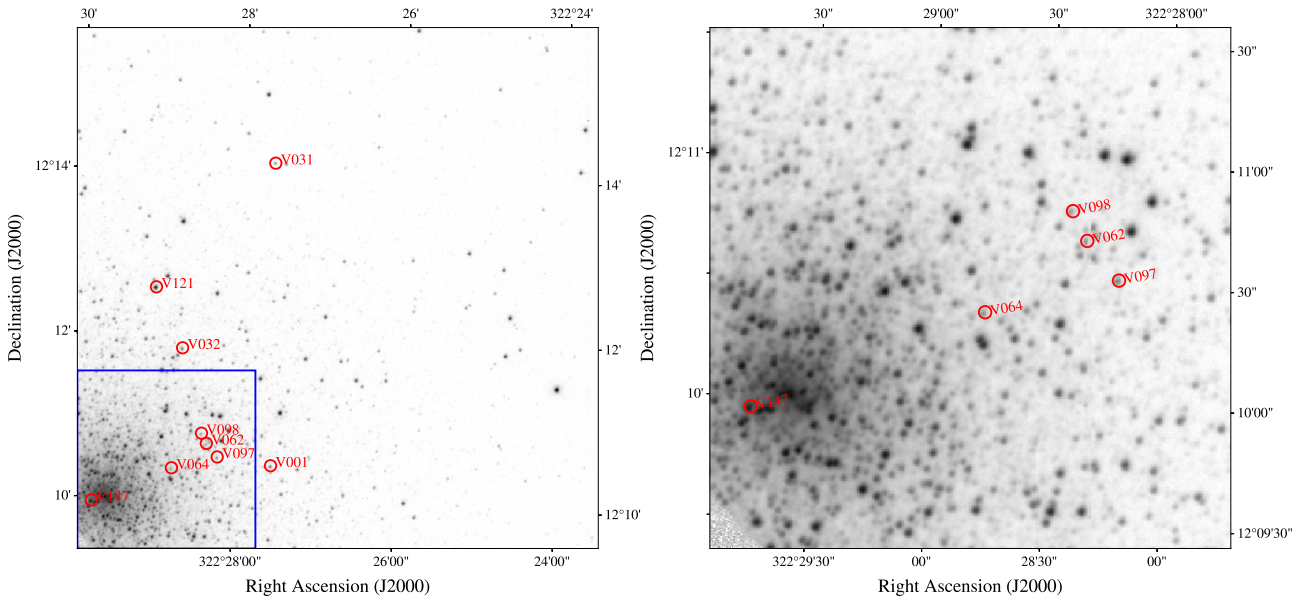


**Figure B13.** Field M15\_4. Conventions are the same as in Figure B10.